Quantum Interference of Unpolarized Single Photons

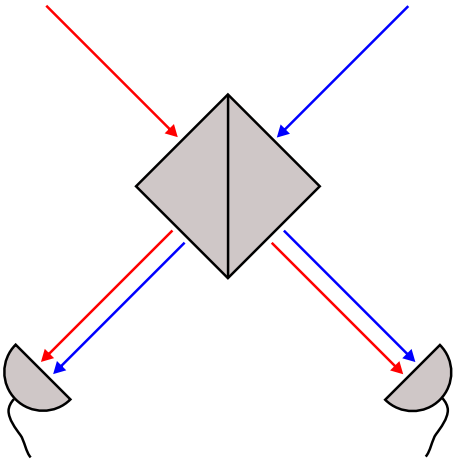

Diplomarbeit

im Studiengang Diplom Physik

angefertigt an der Fakultät für Physik

der Ludwig-Maximilians-Universität München

Arbeitsgruppe Prof. Dr. Harald Weinfurter

von

Christoph Kurz

München, den 15. Juni 2010

Erstgutachter: Prof. Dr. H. Weinfurter
Zweitgutachter: Prof. Dr. M. Christandl

Contents

Chapter 1

Introduction

"Whether you can observe a thing or not depends on the theory which you use. It is the theory which decides what can be observed."

This objection of Albert Einstein during a lecture given by Heisenberg in 1926 [1] expressed his disbelief in quantum mechanics as it was evolving at that time. The Copenhagen interpretation of quantum mechanics, formulated by Bohr and Heisenberg, was no longer a deterministic description of the world, but introduced an element of probability into physics. This gave rise to lively discussions among physicists, since many of them did not believe that quantum mechanics could satisfyingly describe the world. In their famous 1935 paper *"Can Quantum-Mechanical Description of Physical Reality Be Considered Complete?"* [2], Einstein, Podolsky and Rosen (EPR) argued that quantum theory could not be complete. Their gedanken experiment investigated an example for the phenomenon of *entanglement*. Under the assumption of *locality* and *reality*, which EPR thought to be necessary ingredients to any physical theory, they arrived at an apparent contradiction to Heisenberg's uncertainty principle [3]. Hence, they suggested that there should be other theories giving a complete description of reality. Later on, the *local hidden variables* (LHV) theories were introduced. Each particle was attributed experimentally inaccessible parameters determining the outcome of any measurement in advance. Since these hidden variables are unknown, the measurement outcomes remain probabilistic for the observer.

The question if LHV theories are indeed an alternative to quantum mechanics was only philosophical until 1964, when John Bell published the famous inequality named after him [4]. This inequality allows for an experimental discrimination between LHV theories and quantum mechanics by setting a limit for the measurement of correlations between entangled particles. The predictions made by any LHV theory differ from those by quantum mechanics in a such way that LHV theories can be ruled out by violating Bell's inequality. All experimental tests conducted so far are in favor of quantum mechanics [5, 6], but two important aspects must be considered in order to conclusively rule out LHV theories. First, what is known as the *locality loophole* must be closed. If the measurement processes of the two entangled particles are not space-like separated, the first measurement could classically influence the outcome of the second measurement. Second, the *detection loophole* leaves room for some LHV theories if the fraction of all entangled particles that are detected by the measurement process lies below a certain limit [7]. Both loopholes have already been closed separately in the past. Using pairs of entangled photons, strict locality conditions could be ensured [8]. However, due to the high losses of photons, not

all LHV theories could be excluded because of the detection loophole, which was closed in a different experiment. By entangling two trapped atomic ions, a very high read-out efficiency of the quantum states of the ions could be implemented [9, 10], thus closing the detection loophole. Then again, since the ions were trapped on a rather short distance, the condition of locality could not be fulfilled in the same experiment. Hence, no experiment has yet achieved to close both loopholes simultaneously.

A promising route to a loop-hole free test of Bell's inequality is to combine the benefits of the experiments above. The goal of our project is to create entanglement between atoms trapped at remote locations. We aim at a distance of approximately 300 m, which, combined with a sufficiently short time of less than 1 μs needed for the atomic state read-out, allows to close the locality loophole. As the states of the atoms can always be measured, the detection efficiency is intrinsically 1, closing the detection loophole as well. In our setup, we exploit the scheme of *entanglement swapping*. Two single ^{87}Rb atoms are captured in independent traps and subsequently entangled with a photon each. The photons are then distributed over optical fibers and overlapped on a beam splitter in order to perform a *Bell-state measurement* on their joint quantum state. A successful photonic Bell-state projection *heralds* the presence of entanglement between the two atoms [11]. This "event-ready" scheme allows one to analyze every created pair of entangled atoms, which, together with a fast atomic state detection method, will make a first rigorous test of theories based on local hidden variables feasible [12].

In the past, our group demonstrated entanglement between an atom and a photon in the spin degree of freedom [13], followed by the distribution of atom-photon entanglement over an optical fiber link of 300 m length [14]. Meanwhile, a second single-atom trap capable of creating atom-photon entanglement was set up as well [15, 16]. The subject of the present work is the interference of single photons, emitted by two atoms at a distance of 30 m. This interference is the central part of the Bell-state measurement and thus for the creation of entangled pairs of atoms.

Overview

This work starts with the explanation of the basic concepts of entanglement. After reviewing the nature of two-level quantum systems (qubits), the idea of entanglement between two qubits is explained. The Bell states necessary for the Bell-state measurement are introduced before illustrating the scheme of entanglement swapping. The main building block for entangling two remote atoms is, besides two-photon interference, the entanglement of a photon with an atom.

The main chapter deals with the interference of single photons on a non-polarizing fiber beam splitter. The first part consists of the theory of a quantum-optical approach, which allows us to describe the physics involved in two single photons interfering on a beam splitter. The necessary conditions for a successful interference are discussed, the most important point being the indistinguishability of the photons on the beam splitter, on which the fidelity of the prepared entangled atomic state depends. The second, experimental, part concerns the quality of the measured two-photon interference. In principle, there are photonic detection events that are not expected for perfectly interfering wave packets. The presence of these events leads to the conclusion that the wave packets contain more than one photon each.

The last chapter discusses the problem of single atoms emitting more than one photon.

A basic numerical model to describe the probabilities for finding exactly one or more than one photon in a wave packet is developed. These probabilities depend on the properties of the light pulse bringing the atom into the excited state. It will be shown that longer optical excitation pulses result in a higher multi-photon emission probability. These results are then compared to experimental values obtained from a Hanbury-Brown-Twiss measurement. Additional effects, like the multi-level structure of ^{87}Rb, are also discussed since they play a role in the multi-photon emission.

Chapter 2

Concepts of Entanglement

This chapter is an introduction to quantum-mechanical entanglement. It will give an overview of the meaning of entanglement and the role it plays in our experiment. After explaining the basic properties of entangled two-qubit states, the concept of entanglement swapping is presented. We use this in order to create entanglement between two atoms trapped at remote locations. This is done by first entangling each atom with a photon and then interfering the photons on a beam splitter. In this way, a *Bell-state measurement* of the two-photon state can be implemented, creating entanglement between the atoms. We aim to use this to perform a loophole-free test of Bell's inequality.

2.1 Description of two-qubit states

The basic treatment of the state of a quantum-mechanical two-level system will now be given, explaining the meaning of a qubit. Afterwards, the notion of entanglement between two qubits is introduced.

2.1.1 Two-level quantum systems

The state of a quantum-mechanical two-level system $|\Psi\rangle$ is defined as a vector in a two-dimensional Hilbert space. It is the quantum analog of the classical bit, hence the name *qubit*. Examples for two-level systems are the polarization state of a photon or the spin of an electron. Using Dirac notation, the qubit can be in any superposition of two basis states $\{|0\rangle, |1\rangle\}$:

$$|\Psi\rangle = a\,|0\rangle + b\,|1\rangle \tag{2.1}$$

a and b are complex numbers fulfilling the relation $|a|^2 + |b|^2 = 1$ (in other words, the state vector is normalized). A more convenient way to write this is with the use of spherical coordinates:

$$|\Psi\rangle = \cos\frac{\theta}{2}\,|0\rangle + e^{i\phi}\sin\frac{\theta}{2}\,|1\rangle \tag{2.2}$$

with the polar angle θ and the azimuth angle ϕ. In order to understand the relation of this notation to spherical coordinates, we introduce the *Bloch sphere* [17], a visualization of any two-level quantum state. It is a unit sphere, spanned by the eigenstates of the *Pauli operators*. As the quantum-mechanical state is defined over a two-dimensional complex vector space, there are three complementary bases in which the system can be described. Each basis represents the eigenstates of a self-adjoint operator, for which we choose the

Pauli operators $\hat{\sigma}_x$, $\hat{\sigma}_y$, $\hat{\sigma}_z$. In matrix form, with respect to the eigenstates of $\hat{\sigma}_z$, they are given by the Pauli matrices [18]

$$\sigma_x = \begin{pmatrix} 0 & 1 \\ 1 & 0 \end{pmatrix} \tag{2.3}$$

$$\sigma_y = \begin{pmatrix} 0 & -i \\ i & 0 \end{pmatrix} \tag{2.4}$$

$$\sigma_z = \begin{pmatrix} 1 & 0 \\ 0 & -1 \end{pmatrix}. \tag{2.5}$$

These operators constitute non-commuting observables, i.e. they correspond to measurements in complementary bases. If the system is in an eigenstate of one of these observables, measuring it in one of the other bases will yield an entirely random outcome. The eigenstates for $\hat{\sigma}_x$ and $\hat{\sigma}_y$ in terms of the $\hat{\sigma}_z$ eigenbasis are

$$|0_x\rangle = \frac{1}{\sqrt{2}}\left(|0_z\rangle + |1_z\rangle\right) \tag{2.6}$$

$$|1_x\rangle = \frac{1}{\sqrt{2}}\left(|0_z\rangle - |1_z\rangle\right) \tag{2.7}$$

$$|0_y\rangle = \frac{1}{\sqrt{2}}\left(|0_z\rangle + i\,|1_z\rangle\right) \tag{2.8}$$

$$|1_y\rangle = \frac{1}{\sqrt{2}}\left(|0_z\rangle - i\,|1_z\rangle\right). \tag{2.9}$$

The state of the quantum system can now be described by the *Bloch vector* Π, a three-dimensional unit vector whose Cartesian coordinates Π_i are defined as the expectation values of the Pauli operators:

$$\Pi_i = \langle\Psi|\,\hat{\sigma}_i\,|\Psi\rangle \tag{2.10}$$

with $i \in \{x, y, z\}$. The quantum state $|\Psi\rangle$ given in eqn. 2.2 is represented in fig. 2.1, defined in spherical coordinates with radius 1 and angles θ, ϕ.

Depending on the actual physical system, the three complementary bases have different meanings. For the polarization state of a light field, they correspond to linear horizontal/vertical polarization (H/V), linear polarization rotated by 45° (±45°) and circularly polarized light ($\sigma^{\pm}$). In the case of a system with spin $\frac{1}{2}$, for example an electron, the bases correspond to the three spatial axes to which the spin orientation can be parallel or antiparallel.

2.1.2 Notion of entanglement

We now consider a system of n qubits $|\Psi\rangle_i$. For independent qubits, their joint quantum state can be written in form of a product state:

$$|\Psi\rangle = |\Psi\rangle_1 \otimes \cdots \otimes |\Psi\rangle_n \tag{2.11}$$

Such a state is called *separable*. If we cannot find a product representation of $|\Psi\rangle$, the state is *entangled*. This leads to correlations between the qubits, i.e. the outcome of a measurement of the state of a qubit depends on the measurement outcomes of other qubits. Such correlations can arise only if the particles interacted with each other at some point.

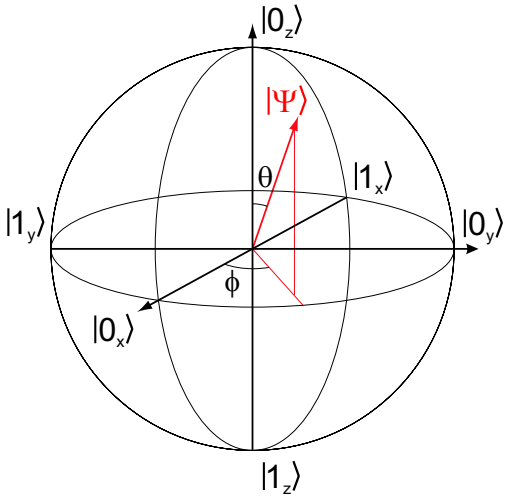

Figure 2.1: Geometric representation of a quantum state $|\Psi\rangle$ on the Bloch sphere, spanned by the axes denoting the eigenstates of the three Pauli operators $\hat{\sigma}_x$, $\hat{\sigma}_y$, $\hat{\sigma}_z$

This interaction can take place either directly (e.g. entangled photons from a down-conversion source, atom-photon entanglement from spontaneous emission) or indirectly (entanglement swapping).

We will confine ourselves to systems of two qubits. This is sufficient to represent our experimental situation, since we are dealing with atom-photon and atom-atom systems. The Hilbert space of a bipartite two-level system has dimension 4, hence we want to find four orthonormal states which form a basis for the Hilbert space. One possibility is to use the non-entangled states $\{|00\rangle, |01\rangle, |10\rangle, |11\rangle\}$ (where $|ij\rangle$ is short for $|i\rangle \otimes |j\rangle$). However, since we will deal with entangled bipartite systems, it is natural to introduce the basis formed by what is called the *Bell states*:

$$\left|\Phi^+\right\rangle = \frac{1}{\sqrt{2}}\left(|00\rangle + |11\rangle\right) \tag{2.12}$$

$$\left|\Phi^-\right\rangle = \frac{1}{\sqrt{2}}\left(|00\rangle - |11\rangle\right) \tag{2.13}$$

$$\left|\Psi^+\right\rangle = \frac{1}{\sqrt{2}}\left(|01\rangle + |10\rangle\right) \tag{2.14}$$

$$\left|\Psi^-\right\rangle = \frac{1}{\sqrt{2}}\left(|01\rangle - |10\rangle\right) \tag{2.15}$$

These states are *maximally entangled*, i.e. the outcome of a measurement of one particle will be completely random. This means that by a *local* measurement, no information about the joint quantum state of the two particles can be obtained. On the other hand, the outcomes of measurements on both particles are strictly correlated. For example, measuring two particles in one of the states $|\Phi^{\pm}\rangle$ will always yield identical outcomes. For particles being in $|\Psi^{\pm}\rangle$, the outcomes are perfectly anticorrelated.

In order to verify that two particles are entangled, it is not sufficient to measure the correlations in a single basis (e.g. the $\hat{\sigma}_z$ basis), but this must be done in at least two complementary bases [19]. This plays a role in confirming entanglement between an atom and a photon or a pair of atoms.

2.1.3 Fidelity

As the last part of the basics of two-level systems, we introduce the fidelity F. It is a measure for the overlap of two quantum states. We use it to estimate the accuracy of an experimentally prepared state, given by its density matrix ρ (see section 4.1.1) with respect to a desired pure state Ψ. The fidelity is then defined as [17]

$$F = \langle\Psi|\,\rho\,|\Psi\rangle\,. \tag{2.16}$$

It simply describes the probability of projecting the state ρ onto the pure state $|\Psi\rangle$ during a measurement. Thus, we find $F = 1$ for the case of a perfectly prepared state.

2.2 Entanglement swapping

Our future goal is to create entanglement between two remote atoms, i.e. atoms in traps separated by a distance of $\approx 300\,\mathrm{m}$. Since there is no way to entangle them by a direct interaction, we must resort to the scheme of entanglement swapping [20].

The general idea of entanglement swapping is the following: let as assume that two independent parties (*Alice* and *Bob*) each have a pair of entangled particles, say Alice's particles are called a and b and Bob's c and d. They both send one of their particles (b and c) to an apparatus performing a *Bell-state measurement* on the joint quantum state of the two particles, that means their state is projected onto one of the four Bell states (see fig. 2.2). As a result of this projective measurement, the other two particles (a and d) shared by Alice and Bob are entangled.

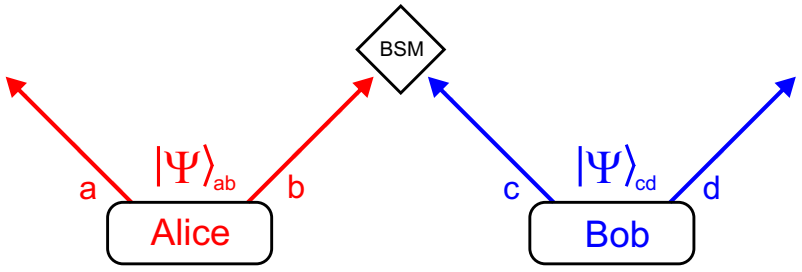

Figure 2.2: Scheme of entanglement swapping. Alice and Bob each have a pair of entangled particles. They contribute one particle each to perform a Bell-state measurement (BSM) on the joint quantum state. Afterwards, the remaining pair of particles, shared by Alice and Bob, is entangled.

Let us consider this process mathematically. Prior to the Bell-state measurement, we assume the particle pairs of Alice and Bob to each be in the Bell state $|\Psi^+\rangle$, since this pertains to our experimental situation (see section 2.3.1). The total quantum state $|\Psi\rangle_{abcd}$ of the four particles is then a product state of Alice's and Bob's pair:

$$|\Psi\rangle_{abcd} = \left|\Psi^+\right\rangle_{ab} \otimes \left|\Psi^+\right\rangle_{cd} \tag{2.17}$$

$$= \frac{1}{\sqrt{2}}\left(|01\rangle + |10\rangle\right)_{ab} \otimes \frac{1}{\sqrt{2}}\left(|01\rangle + |10\rangle\right)_{cd} \tag{2.18}$$

By expanding the brackets and rearranging the order of the particles in the notation, we obtain

$$|\Psi\rangle_{abcd} = \frac{1}{2}\left(|10\rangle_{bc}\,|01\rangle_{ad} + |01\rangle_{bc}\,|10\rangle_{ad} + |11\rangle_{bc}\,|00\rangle_{ad} + |00\rangle_{bc}\,|11\rangle_{ad}\right). \tag{2.19}$$

Since the Bell states form a basis for the Hilbert space, we can rewrite each of the non-entangled states $|ij\rangle$ in terms of the Bell states:

$$|00\rangle = \frac{1}{\sqrt{2}}\left(\left|\Phi^+\right\rangle + \left|\Phi^-\right\rangle\right) \tag{2.20}$$

$$|01\rangle = \frac{1}{\sqrt{2}}\left(\left|\Psi^+\right\rangle + \left|\Psi^-\right\rangle\right) \tag{2.21}$$

$$|10\rangle = \frac{1}{\sqrt{2}}\left(\left|\Psi^+\right\rangle - \left|\Psi^-\right\rangle\right) \tag{2.22}$$

$$|11\rangle = \frac{1}{\sqrt{2}}\left(\left|\Phi^+\right\rangle - \left|\Phi^-\right\rangle\right) \tag{2.23}$$

Inserting this into eqn. 2.19 yields:

$$|\Psi\rangle_{abcd} = \frac{1}{2}\left(\left|\Phi^+\right\rangle_{bc}\left|\Phi^+\right\rangle_{ad} - \left|\Phi^-\right\rangle_{bc}\left|\Phi^-\right\rangle_{ad} + \left|\Psi^+\right\rangle_{bc}\left|\Psi^+\right\rangle_{ad} - \left|\Psi^-\right\rangle_{bc}\left|\Psi^-\right\rangle_{ad}\right) \tag{2.24}$$

Now it can be seen that a projection of the particles b and c onto a Bell state also projects the joint state of the shared pair a and d onto the very same Bell state. Hence, these two particles, in principle being separated by an arbitrary distance, become entangled without ever interacting directly with each other. They did, of course, interact indirectly, since they had to be entangled with b and c, respectively, before these particles were jointly measured.

In our setup, the single atoms in the two traps are each entangled with a photon. The photons are then sent through optical fibers and brought to interference on a beam splitter to perform the Bell-state measurement. These two processes will be treated in more detail later on. After a successful Bell-state measurement, the atoms are entangled in their spin degree of freedom.

2.3 Concept of atom-photon entanglement

The first step towards entangling two remote atoms via entanglement swapping is to entangle each atom with a photon. Each atom is brought to an excited state from where it spontaneously decays via a Λ-type transition, emitting the photon. This is a coherent process when considering the entire atom-photon system. If, in addition, the two possible decay channels are indistinguishable, the two particles become entangled in their spin degree of freedom [13].

2.3.1 Creation of entanglement

In our setup, a single ^{87}Rb atom (nuclear spin $\frac{3}{2}$) is trapped in an optical dipole trap [21]. After preparing the atom in the ground state $^2S_{1/2}\ |F = 1, m_F = 0\rangle$, it is excited via the D_2 transition at a wavelength of 780 nm to the upper state $^2P_{3/2}\ |F' = 0, m_{F'} = 0\rangle$. This state has a mean lifetime of $\tau = 26.23\,\text{ns}$ [22], after which it decays back to one of the ground states. Due to the selection rules, the only possible decay channels are those to the three Zeeman states of the $|F = 1\rangle$ manifold (see fig. 2.3).

As the total angular momentum of the system is conserved, the change of the spin state of the atom results in a corresponding spin state of the photon. This means that

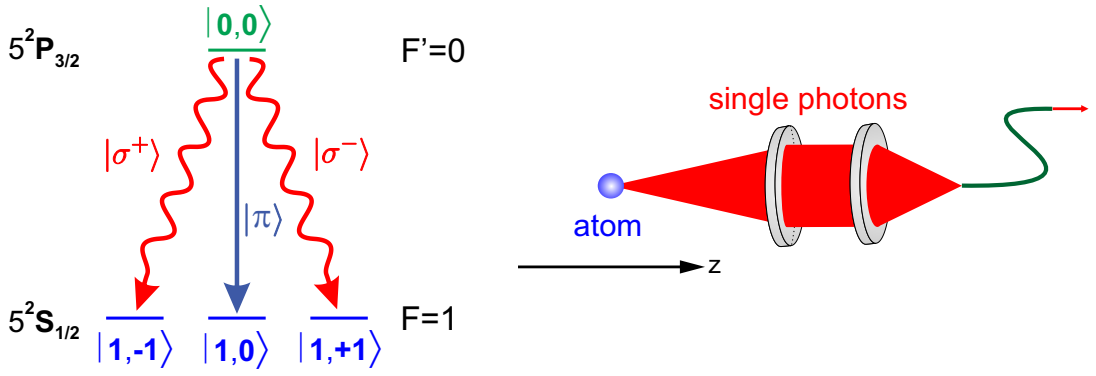

(a) (b)

Figure 2.3: (a) Relevant levels of ^{87}Rb for the creation of atom-photon entanglement. After being excited, the atom decays to one of the ground states via three possible channels. (b) Schematic of the microscope collecting the light from the atom and coupling it into a single-mode optical fiber

a decay to the Zeeman ground state $|m_F = 0\rangle$ leads to a π-polarized photon, while a transition to $|m_F = \pm 1\rangle$ gives a $\sigma^{\mp}$-polarized photon. The amplitudes and relative phases of these three transitions are given by the Clebsch-Gordan coefficients. In our case, they are identical for all decay channels [22]. The three Zeeman states are degenerate in energy, since all external magnetic fields are actively compensated, i.e. the photons emerging from the different channels all have the same frequency. Hence, the only degree of freedom by which the photons can be distinguished are their polarization states. Since the decay of the excited atomic state under the emission of a photon is a coherent process, we obtain the following expression for the atom-photon state:

$$|\Psi\rangle = \frac{1}{\sqrt{3}} \left(|1,-1\rangle \left|\sigma^+\right\rangle + |1,0\rangle |\pi\rangle + |1,+1\rangle \left|\sigma^-\right\rangle \right) \tag{2.25}$$

However, this is not the state which we observe. To collect the light emitted by the atom, we use a microscope which couples the light into a single-mode optical fiber. After passing through the fiber, only the photons emitted in the states $|\sigma^{\pm}\rangle$ are left. This is because the spatial emission function of the π-transition, corresponding to the emission characteristic of a dipole oscillating along the quantization axis (which is defined by the axis of the collection optics), is antisymmteric with respect to the quantization axis. The spatial mode function of the TEM_{00} mode of the fiber, on the other hand, is symmetric with respect to the propagation axis and thus has zero overlap with the wave function of the π-light [23]. The state which we observe after the fiber is then

$$|\Psi\rangle = \frac{1}{\sqrt{2}} \left(|1,-1\rangle \left|\sigma^+\right\rangle + |1,+1\rangle \left|\sigma^-\right\rangle \right). \tag{2.26}$$

2.3.2 Verification of entanglement

The next step is to verify the entanglement between the spin states of the atom and the photon. This is done by measuring the correlation between the polarization of the photon and the spin state of the atom. In order to rule out the possibility of a merely classical correlation, we need to do this in at least two *complementary bases* for the atom-photon state [19]. We choose to analyze the polarization of the photon in the linear

polarization bases $\{|H\rangle, |V\rangle\}$ and $\{|+\rangle, |-\rangle\}$. The horizontal and vertical polarization states are defined as

$$|H\rangle = \frac{1}{\sqrt{2}}\left(\left|\sigma^+\right\rangle + \left|\sigma^-\right\rangle\right) \tag{2.27}$$

$$|V\rangle = \frac{1}{\sqrt{2}}\left(\left|\sigma^+\right\rangle - \left|\sigma^-\right\rangle\right). \tag{2.28}$$

The linear polarization states rotated by 45° with respect to the H/V states are defined as

$$|\pm\rangle = \pm\frac{1}{\sqrt{2}}\, e^{\pm i\frac{\pi}{4}}\left(\left|\sigma^+\right\rangle \mp i\left|\sigma^-\right\rangle\right) \tag{2.29}$$

$$= \pm\frac{1}{\sqrt{2}}\left(|H\rangle \pm i\,|V\rangle\right). \tag{2.30}$$

The corresponding atomic basis states are summarized in tab. 2.1. For example, measuring the photonic polarization to be $|H\rangle$ projects the atom onto the superposition state $\left(|1,+1\rangle + |1,-1\rangle\right)/\sqrt{2}$.

Photonic state	**Atomic state**
$\left\|\sigma^+\right\rangle$	$\|1,-1\rangle$
$\left\|\sigma^-\right\rangle$	$\|1,+1\rangle$
$\|H\rangle$	$\frac{1}{\sqrt{2}}\left(\|1,+1\rangle + \|1,-1\rangle\right)$
$\|V\rangle$	$-\frac{1}{\sqrt{2}}\left(\|1,+1\rangle - \|1,-1\rangle\right)$
$\|+\rangle$	$\frac{1}{\sqrt{2}}\, e^{i\frac{\pi}{4}}\left(\|1,+1\rangle - i\,\|1,-1\rangle\right)$
$\|-\rangle$	$-\frac{1}{\sqrt{2}}\, e^{-i\frac{\pi}{4}}\left(\|1,+1\rangle + i\,\|1,-1\rangle\right)$

Table 2.1: Spin states onto which the atom is projected after measuring the photon to be in the corresponding polarization state

The correlations for a given atomic basis are then obtained by measuring the probability of projecting the atom onto a given basis state after detecting a certain polarization of the photon. For details, refer to [23, 24].

2.3.3 Unpolarized light

A photon entangled with an atom has the peculiar property of being unpolarized, provided the atomic sub-system is not analyzed. When measuring the polarization, we will always obtain both polarization states with equal probability, regardless of the chosen measurement basis. This can be seen as follows: the atom-photon pair is in the maximally entangled state

$$|\Psi\rangle = \frac{1}{\sqrt{2}}\left(|1,-1\rangle\left|\sigma^+\right\rangle + |1,+1\rangle\left|\sigma^-\right\rangle\right). \tag{2.31}$$

With repect to the two-particle basis $\{|1,+1\rangle|\sigma^+\rangle, |1,-1\rangle|\sigma^+\rangle, |1,+1\rangle|\sigma^-\rangle, |1,-1\rangle|\sigma^-\rangle\}$, the density operator of this pure state is then

$$\rho = |\Psi\rangle\langle\Psi| = \frac{1}{2}\begin{pmatrix} 0 & 0 & 0 & 0 \\ 0 & 1 & 1 & 0 \\ 0 & 1 & 1 & 0 \\ 0 & 0 & 0 & 0 \end{pmatrix}. \tag{2.32}$$

Since we are interested only in the state of the photon, we take the partial trace over ρ with respect to the atomic basis:

$$\begin{aligned} \rho_{ph} &= \mathrm{tr}_{\mathrm{at}}\,\rho && (2.33)\\ &= \langle 1,+1|\,\rho\,|1,+1\rangle + \langle 1,-1|\,\rho\,|1,-1\rangle && (2.34)\\ &= \frac{1}{2}\left(|\sigma^+\rangle\langle\sigma^+| + |\sigma^-\rangle\langle\sigma^-|\right), && (2.35) \end{aligned}$$

which is a completely mixed state. The same is, of course, true for the atomic state, i.e. by tracing over the polarization state of the photon, we obtain a completely mixed spin state of the atom. This property of the photon will later on play a role for the Bell-state measurement and entanglement swapping.

Summary

In this section, the notion of atom-photon entanglement was explained. Using a short laser pulse, a single ^{87}Rb atom is transferred to an excited state, from where it spontaneously decays to three possible degenerate Zeeman states. Photons coming from a π-transition are filtered out by a single-mode optical fiber, giving a maximally entangled atom-photon spin state. In order to verify this entanglement, the correlation between the photonic polarization and the atomic spin must be measured. To rule out the possibility of a merely classical correlation, two complementary atomic bases are necessary. A peculiar aspect of the photon, however, is its polarization being in a completely mixed state (which is also true for the atomic spin state), i.e. it is unpolarized. This will play a role in the matter of Bell-state measurement and entanglement swapping.

2.4 Basic principle of two-photon interference

Central to the entanglement swapping scheme is the Bell-state measurement. In our experiment, the goal is to project the joint quantum state of two photons, each entangled with an atom, onto one of the four Bell states. Through this, the atoms become entangled without any direct interaction between them.

Performing a Bell-state measurement on two particles is not easy, since one must take care not to measure the state of only one particle. For us in particular, measuring the polarization state of a photon would project the atom onto a definite state, destroying any entanglement. Each photon is described by a spatio-temporal wave packet. We will see that bringing these wave packets to interference on a 50/50 beam splitter and detecting the photons with single-photon detectors in the outgoing modes of the beam splitter provides a means to distinguish one of the Bell states, namely $|\Psi^-\rangle$, from the other three. In addition, when analyzing the polarization of the photons in the two modes, the state $|\Psi^+\rangle$ can also be discriminated.

We will now give a brief overview of the action of the beam splitter, a more detailed description will follow in section 3.1. The ideal beam splitter is a 50/50 beam splitter, i.e. its reflection and transmission coefficients are equal for any polarization and there are no absorption losses. It has two input modes 1 and 2 from where the photonic wave packets enter. After interfering, they leave via the output modes 3 and 4 (see fig. 2.4).

We describe the number of photons in each mode in terms of the quantum-mechanical creation operator $\hat{c}^\dagger$, which will be explained in more detail in the next chapter. For

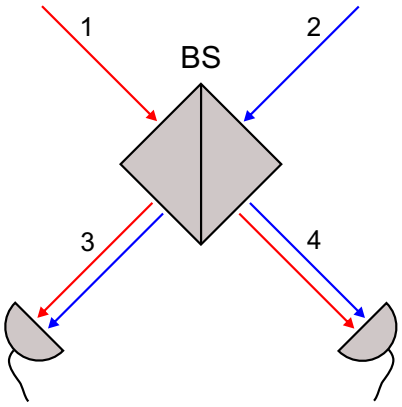

Figure 2.4: Sketch of a beam splitter cube with two incoming and two outgoing spatial modes. In each outgoing mode, a single-photon detector is placed.

example, the operator $\hat{c}^\dagger_{1H}$ creates one photon of horizontal (H) polarization in mode 1. Since the transmission and reflection of the beam splitter is lossless, it must be described by a unitary transformation U, which maps the states of the incoming modes onto the outgoing modes. Additionally, the polarization of a photon is not changed when passing the beam splitter. A transformation fulfilling these requirements is the following:

$$U\left(\hat{c}^\dagger_{1H}\right) = \frac{1}{\sqrt{2}}\left(\hat{c}^\dagger_{3H} + \hat{c}^\dagger_{4H}\right) \tag{2.36}$$

$$U\left(\hat{c}^\dagger_{2H}\right) = \frac{1}{\sqrt{2}}\left(\hat{c}^\dagger_{3H} - \hat{c}^\dagger_{4H}\right) \tag{2.37}$$

$$U\left(\hat{c}^\dagger_{1V}\right) = \frac{1}{\sqrt{2}}\left(\hat{c}^\dagger_{3V} + \hat{c}^\dagger_{4V}\right) \tag{2.38}$$

$$U\left(\hat{c}^\dagger_{2V}\right) = \frac{1}{\sqrt{2}}\left(\hat{c}^\dagger_{3V} - \hat{c}^\dagger_{4V}\right) \tag{2.39}$$

We will choose the basis $\{H, V\}$ of horizontal and vertical polarization for the photons. Because we decided to use the *second quantization* [25], we write the photonic states in terms of the number state representation. For example, a photon of horizontal polarization in mode 1 is described by the quantum state $|1_{1H}\rangle = \hat{c}^\dagger_{1H}|0\rangle$, where the indices denote the spatial mode and polarization, respectively, while $|0\rangle$ is the vacuum state. The four Bell states for the incoming photons can then be rewritten in the following form:

$$\left|\Phi^\pm\right\rangle = \frac{1}{\sqrt{2}}\left(|HH\rangle \pm |VV\rangle\right) \tag{2.40}$$

$$= \frac{1}{\sqrt{2}}\left(|1_{1H}1_{2H}\rangle \pm |1_{1V}1_{2V}\rangle\right) \tag{2.41}$$

$$\left|\Psi^\pm\right\rangle = \frac{1}{\sqrt{2}}\left(|HV\rangle \pm |VH\rangle\right) \tag{2.42}$$

$$= \frac{1}{\sqrt{2}}\left(|1_{1H}1_{2V}\rangle \pm |1_{1V}1_{2H}\rangle\right) \tag{2.43}$$

The next step is to write these states in terms of the creation operators. For the states

$|\Phi^{\pm}\rangle$, we obtain

$$\left|\Phi^{\pm}\right\rangle = \frac{1}{\sqrt{2}}\left(|1_{1H}1_{2H}\rangle \pm |1_{1V}1_{2V}\rangle\right) \tag{2.44}$$

$$= \frac{1}{\sqrt{2}}\left(\hat{c}^{\dagger}_{1H}\,\hat{c}^{\dagger}_{2H}\,|0\rangle \pm \hat{c}^{\dagger}_{1V}\,\hat{c}^{\dagger}_{2V}\,|0\rangle\right). \tag{2.45}$$

We then apply the beam splitter transformation U on the creation operators for the incoming modes. After simplification, the transformed state is

$$U\left(\left|\Phi^{\pm}\right\rangle\right) = \frac{1}{2\sqrt{2}}\left[\left(\hat{c}^{\dagger}_{3H}\right)^2 - \left(\hat{c}^{\dagger}_{4H}\right)^2 \pm \left(\hat{c}^{\dagger}_{3V}\right)^2 \mp \left(\hat{c}^{\dagger}_{4V}\right)^2\right]|0\rangle \tag{2.46}$$

$$= \frac{1}{2}\left(|2_{3H}\rangle - |2_{4H}\rangle \pm |2_{3V}\rangle \mp |2_{4V}\rangle\right). \tag{2.47}$$

This is a superposition of states where both photons are in the same outgoing mode and identically polarized. Hence, they will always impinge on the same single-photon detector. Since our detectors cannot resolve the number of photons in a wave packet triggering a detection event, the Bell states $|\Phi^{\pm}\rangle$ appear to be single-photon events. This is why we cannot distinguish these states from the other two Bell states or single-photon events with the simple setup sketched in fig. 2.4.

The same calculation can be done for the states $|\Psi^{\pm}\rangle$. After writing the states in terms of the creation operators and applying the beam splitter transformation, we obtain

$$U\left(\left|\Psi^{+}\right\rangle\right) = \frac{1}{\sqrt{2}}\left(|1_{3H}1_{3V}\rangle - |1_{4H}1_{4V}\rangle\right) \tag{2.48}$$

$$U\left(\left|\Psi^{-}\right\rangle\right) = \frac{1}{\sqrt{2}}\left(|1_{3V}1_{4H}\rangle - |1_{3H}1_{4V}\rangle\right). \tag{2.49}$$

As one can see, the photons still leave the beam splitter in the same spatial mode for the $|\Psi^{+}\rangle$ state. By placing one detector in each outgoing mode, it is still not possible to detect this state, since it will cause a single-photon event in one of the detectors. However, the situation is different for the state $|\Psi^{-}\rangle$, because it will trigger *coincident* detection events in the two single-photon detectors. This means that coincident clicks in the detectors announce the projection of the joint photonic state onto the Bell state $|\Psi^{-}\rangle$. With a more sophisticated setup analyzing also the polarizations of the photons in the outgoing modes of the beam splitter, the state $|\Psi^{+}\rangle$ can be distuingished as well (see section 3.1.2).

This measurement scheme makes it possible to project the joint photonic polarization state onto two of the four Bell states. As we are dealing with unpolarized photons (cf. section 2.3.3), the procedure succeeds in 50 % of all cases. For the other two states, only single-photon events are detected (a complete Bell-state analysis was demonstrated in [26]). However, these calculations assume the ideal case of perfect interference on the beam splitter. This means that the photonic wave packets are identical in their temporal shape and frequency and that they overlap perfectly (spatially and temporally) on the beam splitter. The more general case of interfering photons of different frequencies and with imperfect overlap will be treated in detail in section 3.1.

2.5 Test of Bell's inequality

Quantum mechanics has been able to successfully describe all experimental observations in physics so far. Yet one of its characteristics is the randomness inherent in the measurement

process. Before a specific property of a quantum system is measured, this property is undefined: it can be in a linear superposition or an incoherent mixture of the basis states of the measured observable. Moreover, the notion of entanglement gives rise to the conclusion that quantum mechanics does not allow for a *local* description of a system. For a maximally entangled two-particle system, for example, the quantum state of each particle is undefined, while the combined system is in a pure state.

With the lack of the fundamental ideas of *reality* and *locality* in quantum mechanics, Einstein, Podolsky and Rosen were the first to propose an alternative class of theories, namely the *local hidden variable* (LHV) theories [2]. These make the assumption that a particle carries hidden (experimentally inaccessible) information determining the outcome of a measurement. At first, this was merely a philosophical question as there was no experimental way to distinguish between quantum mechanics and LHV theories, until John Bell derived an inequality making different predictions for the two theories [4]. He considered two entangled spin-$\frac{1}{2}$ particles a and b which are sent to remote locations. The spin state of each particle is then measured in different bases. The spin of particle a is measured under an angle α with respect to the quantization axis and particle b under an angle β. The outcome of each measurement can take the values ± 1. Let us denote by $\langle \sigma_\alpha \otimes \sigma_\beta \rangle$ the expectation value of the joint measurement of the particles under the angles α and β. Bell's inequality in the CHSH formulation [27] then takes the form

$$S := |\langle \sigma_\alpha \otimes \sigma_\beta \rangle + \langle \sigma_{\alpha'} \otimes \sigma_\beta \rangle| + \left| \langle \sigma_\alpha \otimes \sigma_{\beta'} \rangle - \langle \sigma_{\alpha'} \otimes \sigma_{\beta'} \rangle \right| \leq 2 \tag{2.50}$$

for any choice of the measurement bases α, α', β, β'. Any LHV theory should fulfill this inequality. However, quantum mechanics predicts a different bound for the values of S, namely

$$S \leq 2\sqrt{2}. \tag{2.51}$$

For a maximally entangled state and suitable choices of the measurement bases, the value $S = 2\sqrt{2}$ can be obtained, violating Bell's inequality. Thus we have a means to rule out any theory based on local hidden variables by performing appropriate measurements on a pair of entangled particles.

Loopholes

In order to eliminate all LHV theories, it is not sufficient to simply violate Bell's inequality as described above, as there are two *loopholes* which must be addressed:

a) **Locality loophole**: it is necessary to measure the quantum states of the two particles independently. This means that the measurement of each particle must be completed before any information about the measurement outcome of the other particle can be received (space-like separation). Additionally, the choice of the measurement basis of each particle must be random and independent of the basis choice for the other particle.

b) **Detection loophole**: experimentally, not all particles can be measured. Therefore we must assume the detected fraction to be representative for all entangled pairs of particles (*fair sampling assumption*). For conclusive results, a sufficiently large fraction must be read out [28]. In our case of a maximally entangled state, the necessary detection efficiency for each particle amounts to 82.8 % [12].

Both loopholes have already been closed separately in the past. The locality loophole was overcome by using pairs of entangled photons [8]. The photons, originating from a down-conversion source, were distributed to remote locations through optical fibers and then locally measured in polarization bases independently and randomly chosen by quantum random number generators. However, the fraction of detected photon pairs was far too small to close the detection loophole, which was done in a different experiment. Using the entanglement swapping scheme, a pair of Yb^+ ions was entangled in the spin degree of freedom [9]. As reading out the state of an ion always yields a result, the detection loophole was closed. Still, the problem of the locality loophole could not be solved, as the ions had only a distance of $\approx 1\,\mathrm{m}$.

With our setup, the aim for the future is to create entanglement between two atoms at a distance of $\approx 300\,\mathrm{m}$. By implementing a fast detection technique to read out the atomic states [29], it should be feasible to close both the locality and the detection loophole in the same experiment [12].

Summary

In this chapter, the concepts of quantum-mechanical entanglement and its role for our experiment were introduced. The properties of two-level quantum systems (qubits) were reviewed. The state of a qubit can be represented as a three-dimensional vector on the Bloch sphere, given by the three Pauli operators. The sets of eigenstates of the Pauli operators each form an orthonormal basis for the two-level Hilbert space.

A system of two qubits can show the non-classical behavior of entanglement, manifesting itself in correlations between the outcomes of measurements of the two particles. A natural basis for this two-qubit Hilbert space are the maximally entangled Bell states. They play an important role in the process of entanglement swapping, which allows for entangling two particles without the need for them to interact directly. In our setup, we first create entanglement between an atom and a photon in the spin degree of freedom by exploiting the nature of the atomic spontaneous decay. This is done for two atom-photon pairs, from which the photons are brought to interference on a non-polarizing beam splitter. By measuring coincident detection events in the outgoing spatial modes of the beam splitter, the two-photon state can be projected onto two out of four Bell states, performing a Bell-state measurement. This projects the system of the two atoms onto a maximally entangled state, completing the entanglement swapping scheme.

The long-term goal of our experiment is to use pairs of entangled atoms in order to violate Bell's inequality with the locality and detection loophole closed simultaneously. This will then allow us to rule out all local hidden variable theories.

Chapter 3

Quantum Interference of Single Photon Pairs

In the previous chapter, we gave an insight into the idea of entanglement swapping and two-photon interference. We will now go into detail how interference of two photons emitted by independent atoms can be achieved.

The first part of this chapter explains the theory needed to fully describe the interference of two independent photons on a beam splitter and which experimental parameters can be adjusted for successful entanglement swapping. The second part describes the experimental requirements and the measurement results.

3.1 Theory of two-photon interference

We will investigate how a Bell-state measurement of two photons can be done in order to perform the entanglement swapping. We can do this by having the photons interfere on a 50/50 beam splitter, projecting the two-photon state onto one of the four Bell states with a success probability of 25 %.

In this section, a full quantum-mechanical treatment of the beam splitter and the photonic wave packets impinging on it will be given. The fidelity of the measured photonic state with respect to the theoretical Bell state depends on a number of factors, such as the temporal shape of the wave packets, the difference in frequency and arrival time of the photons, the detection time window and the beam splitter itself. We will see that only for ideal conditions, i.e. a perfect 50/50 beam splitter and identical wave packets arriving simultaneously, is the fidelity 1. On the way there, we will discuss the probability of detecting a coincidence in the photon detectors as a function of above parameters.

The necessary calculations follow mainly the line of [30] and can be found there in more detail.

3.1.1 Quantum-mechanical description of the light field

As we are dealing with light fields containing only single photons, the classical description of light is no longer sufficient. We will exploit the fact that a light wave can be decomposed into plane waves. At a fixed point in space, each of these is equivalent to a harmonic oscillator [31]. We will therefore resort to describing our photonic wave packets in terms

of the quantum-mechanical harmonic oscillator. For a given frequency ω of a plane wave, the Hamiltonian reads

$$\hat{H} = \hbar\omega \left(\hat{a}_\varepsilon^\dagger(\omega)\, \hat{a}_\varepsilon(\omega) + \frac{1}{2} \right) \tag{3.1}$$

with $\hat{a}_\varepsilon^\dagger(\omega)$ and $\hat{a}_\varepsilon(\omega)$ being the creation and annihilation operator, respectively. These operators create and destroy photons per unit frequency with polarization $\varepsilon \in \{H, V\}$ in the light mode ω and obey the commutation relation

$$\left[\hat{a}_\varepsilon(\omega), \hat{a}_{\varepsilon'}^\dagger(\omega') \right] = \delta_{\varepsilon\varepsilon'}\, \delta(\omega - \omega'). \tag{3.2}$$

Using the creation operator $\hat{a}_\varepsilon^\dagger$, any number of photons can be added to the vacuum state $|0\rangle$. The mode of the light field can thus be occupied by an arbitrary number of photons. This number is given by the number density operator

$$\hat{N}_\varepsilon(\omega) = \hat{a}_\varepsilon^\dagger(\omega)\, \hat{a}_\varepsilon(\omega). \tag{3.3}$$

This operator describes the number of photons per unit frequency of a light field and will later on play a role in the context of photon detection. We also want to define creation and annihilation operators for wave packets containing a spectrum of frequencies. Given the spectral amplitude $\chi(\omega)$ of a wave packet, we may set

$$\hat{c}_\varepsilon^{(\dagger)} = \int \chi(\omega)\, \hat{a}_\varepsilon^{(\dagger)}(\omega)\, \mathrm{d}\omega. \tag{3.4}$$

These operators may now be used to describe a light field composed of an an entire spectrum of frequencies (where the probability density of the spectrum is given by $|\chi(\omega)|^2$). The according commutation relation reads

$$\left[\hat{a}_\varepsilon(\omega), \hat{c}_{\varepsilon'}^\dagger \right] = \delta_{\varepsilon\varepsilon'}\, \chi(\omega). \tag{3.5}$$

Temporal description of a light field

Having the tools to describe a wave packet in frequency space, we can go to the time domain by simply taking the Fourier transform of all functions and operators. For a fixed point in space, which we set to be $z = 0$, we obtain:

$$\hat{a}_\varepsilon^{(\dagger)}(t) = \frac{1}{\sqrt{2\pi}} \int \hat{a}_\varepsilon^{(\dagger)}(\omega)\, e^{-i\omega t}\, \mathrm{d}\omega \tag{3.6}$$

$$\chi(t) = \frac{1}{\sqrt{2\pi}} \int \chi(\omega)\, e^{-i\omega t}\, \mathrm{d}\omega \tag{3.7}$$

The operators $\hat{a}_\varepsilon^{(\dagger)}(t)$ now describe the light field in the time domain, i.e. they create and destroy photons per unit time. The function $\chi(t)$ is simply the temporal amplitude of the wave packet. The intensity $I(t)$ of the light field is then proportional to $|\chi(t)|^2$. The number density operator thus gives the number of photons per unit time:

$$\hat{N}_\varepsilon(t) = \hat{a}_\varepsilon^\dagger(t)\, \hat{a}_\varepsilon(t) \tag{3.8}$$

In analogy to eqn. 3.4, the operators describing the entire light field are given by

$$\hat{c}_{\varepsilon}^{(\dagger)} = \int \chi(t)\, \hat{a}_{\varepsilon}^{(\dagger)}(t)\, \mathrm{d}t. \tag{3.9}$$

The commutation relations behave accordingly:

$$\left[\hat{a}_{\varepsilon}(t), \hat{a}_{\varepsilon'}^{\dagger}(t')\right] = \delta_{\varepsilon\varepsilon'}\, \delta(t - t') \tag{3.10}$$

$$\left[\hat{a}_{\varepsilon}(t), \hat{c}_{\varepsilon'}^{\dagger}\right] = \delta_{\varepsilon\varepsilon'}\, \chi(t) \tag{3.11}$$

3.1.2 Action of a beam splitter

Seeing how the creation and annihilation operators of the quantum-mechanical oscillator describe a light field, we can now use these to investigate the effect of a beam splitter. It is important to notice that the fraction of transmitted and reflected light is in general not the same and also depends on the polarization. We will therefore introduce the transmittances h and v for horizontal and vertical polarization, respectively. As the absorption of the beam splitter should be negligible, it can be described by a unitary transformation U. One possible choice for this is a generalized form of eqns. 2.36 - 2.39 for a non-perfect beam splitter:

$$U\left(\hat{c}_{1H}^{\dagger}\right) = \sqrt{1-h}\, \hat{c}_{3H}^{\dagger} + \sqrt{h}\, \hat{c}_{4H}^{\dagger} \tag{3.12}$$

$$U\left(\hat{c}_{2H}^{\dagger}\right) = \sqrt{h}\, \hat{c}_{3H}^{\dagger} - \sqrt{1-h}\, \hat{c}_{4H}^{\dagger} \tag{3.13}$$

$$U\left(\hat{c}_{1V}^{\dagger}\right) = \sqrt{1-v}\, \hat{c}_{3V}^{\dagger} + \sqrt{v}\, \hat{c}_{4V}^{\dagger} \tag{3.14}$$

$$U\left(\hat{c}_{2V}^{\dagger}\right) = \sqrt{v}\, \hat{c}_{3V}^{\dagger} - \sqrt{1-v}\, \hat{c}_{4V}^{\dagger} \tag{3.15}$$

The indices denote the spatial mode and the polarization. The square roots over the transmission and reflection coefficients arise from the fact that the operators describe amplitudes and not intensities. U is, of course, a linear transformation since the beam splitter is a linear optical element, i.e. the transformation of a superposition of some input states is given by the respective superposition of their transformation.

From now on, we will treat the Bell state $|\Psi^-\rangle$ as the one onto which we wish to project the joint photonic state, because this is the easiest to distinguish from the other Bell states (since this is the only state for which the photons leave the beam splitter separately, cf. eqn. 2.49). Nonetheless, the state $|\Psi^+\rangle$ can by analyzed as well. This is done by performing a polarization measurement in the two outgoing modes by placing two polarizing beam splitters behind the normal beam splitter (see fig. 3.1(a)). Two photons in the $|\Psi^+\rangle$ state leave the beam splitter together but will then be separated by one of the PBS as they have orthogonal polarizations. Hence, they will cause a coincidence in a detector pair behind one of the PBS.

When analyzing the $|\Psi^-\rangle$ state, we look for coincidences in the outgoing modes of the beam splitter, regardless of the polarization analyses. A coincidence between the detector pairs behind the two PBS then announces the projection onto $|\Psi^-\rangle$. For $|\Psi^+\rangle$, however, since a projection onto $|\Psi^+\rangle$ is given by a coincidence between the detectors analyzing the horizontal and those analyzing the vertical polarization states, we look for

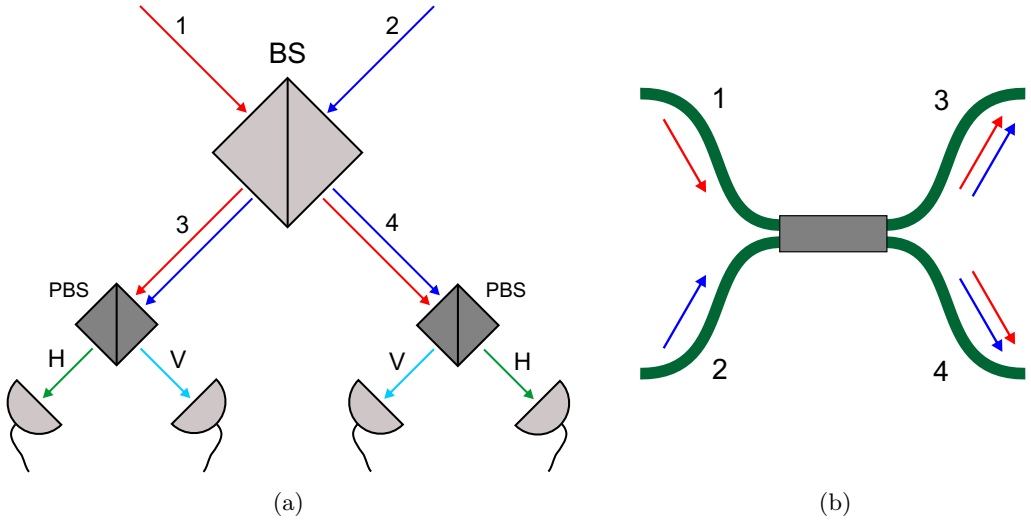

(a) (b)

Figure 3.1: (a) Schematic of a beam splitter (BS) cube with input modes 1 and 2 and output modes 3 and 4. A coincidence in the two output modes projects the two-photon state onto $|\Psi^-\rangle$. Performing polarization analyses with two polarizing beam splitters detects also $|\Psi^+\rangle$, as for this state, the photons have orthogonal polarizations and will cause coincident detection events behind one of the PBS. (b) Schematic of a fiber beam splitter. The four spatial modes now propagate through four fiber pigtails, each of which changing the polarization state of the light due to their birefringence.

coincidences in polarization instead of spatial mode. Hence, the mathematical treatment of these states is completely analogous and we will confine ourselves to describing the Bell-state measurement for the $|\Psi^-\rangle$ state.

Fiber beam splitter

In our setup, we do not use a free-space beam splitter cube but a fiber beam splitter (see fig. 3.1(b)). It basically consists of two fibers brought together in the middle. The light propagating through one of the fibers then "leaks" to the other via its evanescent field. This can be engineered quite precisely such that the contact point acts as a good 50/50 beam splitter. The advantage of this kind of beam splitter is the perfect spatial overlap of the modes in the fibers, which is also much less sensitive to vibrations and thermal expansion compared to the free-space case.

Yet this solution has a drawback, namely the birefringence of the four fiber pigtails. This leads to unitary tranformations of the polarization states of the photons. We adjust the birefringence of a fiber pigtail by a manual polarization controller, consisting of three small plates in which the fiber is bent to loops. By rotating the loops relative to each other, the stress of the fiber is varied, changing its birefringence. In this way, the polarization of the light in the fiber can be varied in an arbitrary way. In particular, it is possible to neutralize the birefringence such that the polarization is maintained.

Experimentally, this is done by sending light of two different polarizations (e.g. $|V\rangle$ and $|+\rangle$) through the fiber and optimizing the birefringence until both polarizations are maintained. Then the fiber can be used for light polarized in any basis without transforming its state.

As we cannot disassemble the beam splitter, it is not possible to compensate for the birefringence of each fiber pigtail separately. However, this is not necessary; for the entanglement swapping scheme, all we need is the same unitary transformation of the polarization along each of the four possible paths through the beam splitter. Experimentally, we achieve this by neutralizing the birefringence along each path by in the following order:

1. Maintain the polarization along the path through the fibers 1 and 3 by adjusting the birefringence of one (or both) of the fibers
2. Maintain the polarization along the path through the fibers 1 and 4 by adjusting the birefringence of fiber 4
3. Maintain the polarization along the path through the fibers 2 and 3 by adjusting the birefringence of fiber 2

Optimizing these three paths for all polarization bases is a rather time-consuming process, but a simplification arises when observing only two-photon interference: since the photons in the incoming fibers are unpolarized, the birefringence of these two fibers is irrelevant. The only requirement is that the two outgoing fibers perform the same unitary operation on the polarization states. This means that we can omit step 3 in the compensation procedure above.

3.1.3 Photon detection

So far we have developed a toolbox for the quantum-mechanical description of a light field and its transformation by a beam splitter. The missing part for completing the Bell-state measurement is the effect of photon detection by the single-photon detectors. We will investigate this effect now for the single- as well as the two-photon detection.

Single-photon detection

Let us consider a light field in an arbitrary quantum state $|i\rangle$ incident on a single-photon detector with quantum efficiency η. The photon number per unit time propagating through the mode is given by the number density operator $\hat{N}_\varepsilon(t)$, defined in eqn. 3.8. The probability of detecting a photon in the time interval $[t, t+\mathrm{d}t]$ is then

$$\begin{aligned} p_i^{(1)}(t)\,\mathrm{d}t &= \eta \sum_\varepsilon \langle i|\, \hat{N}_\varepsilon(t)\, |i\rangle\,\mathrm{d}t && (3.16)\\ &= \eta \sum_\varepsilon \langle i|\, \hat{a}_\varepsilon^\dagger(t)\, \hat{a}_\varepsilon(t)\, |i\rangle\,\mathrm{d}t && (3.17)\\ &= \eta\, G_i^{(1)}(t)\,\mathrm{d}t && (3.18) \end{aligned}$$

with the first-oder correlation function with respect to the initial state $|i\rangle$

$$G_i^{(1)}(t) = \sum_\varepsilon \langle i|\, \hat{a}_\varepsilon^\dagger(t)\, \hat{a}_\varepsilon(t)\, |i\rangle\,. \qquad (3.19)$$

This function is a measure for the total number of photons (as we sum over all polarization states n) per unit time in the light state $|i\rangle$.

Two-photon detection

Since we are interested in the probability of a coincidence of photon detections in two different detectors, we extend the above case to the probability of detecting *two* photons of a given light state $|i\rangle$. Assuming the detectors (efficiencies η_1 and η_2) are at the same distance from the beam splitter (which is a very good approximation in our case), the probability of detecting a photon in output mode 3 in the time interval $[t_1, t_1 + \mathrm{d}t_1]$ and another photon in output mode 4 in the time interval $[t_2, t_2 + \mathrm{d}t_2]$ is given by the respective number density operators:

$$p_i^{(2)}(t_1,t_2)\,\mathrm{d}t_1\mathrm{d}t_2 = \eta_1\eta_2 \sum_{\varepsilon,\varepsilon'} \langle i|\,\hat{N}_{3\varepsilon}(t_1)\,\hat{N}_{4\varepsilon'}(t_2)\,|i\rangle\,\mathrm{d}t_1\mathrm{d}t_2 \tag{3.20}$$

$$= \eta_1\eta_2 \sum_{\varepsilon,\varepsilon'} \langle i|\,\hat{a}^\dagger_{3\varepsilon}(t_1)\,\hat{a}^\dagger_{4\varepsilon'}(t_2)\,\hat{a}_{3\varepsilon}(t_1)\,\hat{a}_{4\varepsilon'}(t_2)\,|i\rangle\,\mathrm{d}t_1\mathrm{d}t_2 \tag{3.21}$$

$$= \eta_1\eta_2\, G_i^{(2)}(t_1,t_2)\,\mathrm{d}t_1\mathrm{d}t_2 \tag{3.22}$$

We defined the second-order correlation function with respect to the state $|i\rangle$ as

$$G_i^{(2)}(t_1,t_2) = \sum_{\varepsilon,\varepsilon'} \langle i|\,\hat{a}^\dagger_{3\varepsilon}(t_1)\,\hat{a}^\dagger_{4\varepsilon'}(t_2)\,\hat{a}_{3\varepsilon}(t_1)\,\hat{a}_{4\varepsilon'}(t_2)\,|i\rangle\,. \tag{3.23}$$

This function can now be used for correlating the expectation values for photon numbers in two modes at different points in time. It is a natural way to calculate the coincidence probability of two photons in different modes.

The roadmap for the description of two-photon interference on a beam splitter is then to find an expression for $G_i^{(2)}(t_1,t_2)$ for a given state of the light field behind the beam splitter. This state can be deduced from the incoming modes using the temporal shapes of the wave packets and the transformation by the beam splitter.

3.1.4 Coincidence probabilities for the Bell states

In the following, we will calculate the second-order correlation function for given temporal shapes $\chi_1(t)$ and $\chi_2(t)$ of the incoming wave packets. For convenience, we redefine the notation of the correlation function as

$$G_{f_i}^{(2)}(t_1,t_2) \to G_i^{(2)}(t_1,t_2)\,, \tag{3.24}$$

where $|f_i\rangle$ is the transformation of the initial state $|i\rangle$ by the beam splitter. For example, $G_{HH}^{(2)}(t_1,t_2)$ denotes the second-order correlation function for the state originating from the transformation of the state $|HH\rangle$ *before* the beam splitter.

First, we will consider the Bell states $|\Phi^\pm\rangle$ for the incoming light, which are superpositions of the states $|HH\rangle$ and $|VV\rangle$. In general, the second-order correlation function of a superposition of two states is not simply the sum of the separate correlation functions. However, for $|\Phi^\pm\rangle$, the cross-terms arising from the sum in eqn. 3.23 vanish:

$$\langle f_{VV}|\,\hat{a}^\dagger_{3\varepsilon}(t_1)\,\hat{a}^\dagger_{4\varepsilon'}(t_2)\,\hat{a}_{3\varepsilon}(t_1)\,\hat{a}_{4\varepsilon'}(t_2)\,|f_{HH}\rangle = 0 \tag{3.25}$$

for all polarizations ε and ε'. It follows

$$G_{\Phi^\pm}^{(2)} = \frac{1}{2}\left(G_{HH}^{(2)} + G_{VV}^{(2)}\right). \tag{3.26}$$

It is a rather lengthy, but straightforward, calculation to evaluate this expression. The result for the correlation functions, after using eqn. 3.11 and applying the beam splitter transformation, is given by

$$G^{(2)}_{HH}(t_1,t_2) = |h\,\chi_1(t_1)\,\chi_2(t_2) - (1-h)\,\chi_1(t_2)\,\chi_2(t_1)|^2 \tag{3.27}$$

$$G^{(2)}_{VV}(t_1,t_2) = |v\,\chi_1(t_1)\,\chi_2(t_2) - (1-v)\,\chi_1(t_2)\,\chi_2(t_1)|^2 . \tag{3.28}$$

It is interesting to note that for the $|\Phi^{\pm}\rangle$ states, the second-order correlation function and by that the coincidence probability can be derived independently from the parts $|HH\rangle$ and $|VV\rangle$ of the states, i.e. no interference between these components takes place. This is different for the $|\Psi^{\pm}\rangle$ states, where an additional interference term shows up:

$$G^{(2)}_{\Psi^{\pm}} = \frac{1}{2}\left(G^{(2)}_{HV} + G^{(2)}_{VH} \pm 2\sum_{\varepsilon\neq\varepsilon'} K_{\varepsilon,\varepsilon'}\right) \tag{3.29}$$

The non-interfering parts are symmetric and given by

$$G^{(2)}_{HV}(t_1,t_2) = G^{(2)}_{VH}(t_1,t_2) = h\,v\,|\chi_1(t_1)\,\chi_2(t_2)|^2 + (1-h)\,(1-v)\,|\chi_1(t_2)\,\chi_2(t_1)|^2 , \tag{3.30}$$

while for the interference term we find

$$\sum_{\varepsilon\neq\varepsilon'} K_{\varepsilon,\varepsilon'}(t_1,t_2) = -2\sqrt{h\,v\,(1-h)\,(1-v)}\,\mathrm{Re}\left[\chi_1(t_1)\,\chi_2(t_2)\,\chi_1^*(t_2)\,\chi_2^*(t_1)\right] . \tag{3.31}$$

Photon detection without time resolution

We briefly consider the case of detectors whose time-resolution is much worse than the duration of the photonic wave packets. In this case, the detectors cannot properly resolve the time difference between two detection events and all events of which the time difference lies within the detection resolution will be treated as a coincidence. This leads to what is called the Hong-Ou-Mandel effect [32]. The probability for a coincidence is then given by integrating over eqn. 3.22:

$$P^{(2)}_i = \eta_1\eta_2 \iint G^{(2)}_i(t_1,t_2)\,\mathrm{d}t_1\mathrm{d}t_2 \tag{3.32}$$

However, this case does not apply to our setup, since our photon detectors have a time resolution of better than 1 ns, which is much smaller than the typical duration of the wave packets given by the lifetime $\tau = 26.23\,\mathrm{ns}$ of the upper atomic state.

Time-resolved photon detection

For the following calculations, we need to know the actual temporal form of the photonic wave packets arriving at the beam splitter. The probability density $|\chi(t)|^2$ can be measured experimentally by repeatedly exciting an atom and recording the arrival times of the photons at the detectors. A typical time histogram is shown in fig. 3.2.

We approximate the shape of our photons by the exponential decay, neglecting the part arising from the excitation. This is justified for sufficiently short pulses. For a fixed point in space, the temporal shape is then given by

$$\chi(t) = \frac{1}{\sqrt{\tau}}\,e^{-\frac{1}{2}\frac{t-t_0}{\tau}}\,\Theta(t-t_0)\,e^{-i\omega_0 t} \tag{3.33}$$

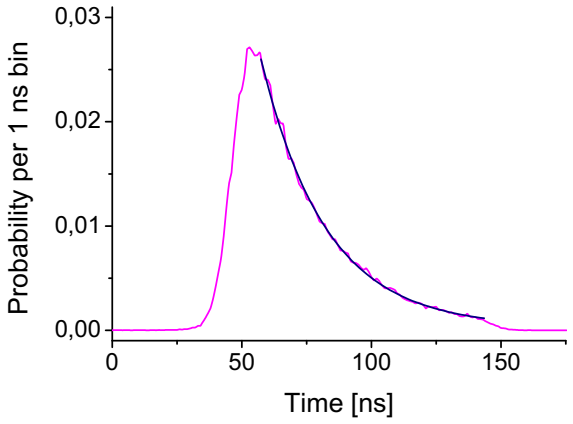

Figure 3.2: Histogram of the arrival times of single photons emitted by an atom which is repeatedly excited. From the exponential fit, the lifetime of the upper atomic state can be inferred to $\tau = 25.1 \pm 0.2\,\mathrm{ns}$.

with Θ being the Heaviside step function. The parameters characterizing the wave packet are the arrival time at the beam splitter t_0, the light angular frequency ω_0 and the atomic lifetime τ. In the following, we can assume τ and ω_0 to be identical for both photons entering the beam splitter, as they are emitted by the same atomic species. From the temporal shape, the frequency spectrum of the wave packet as well as the arrival times of two independent photons can be calculated (see appendix A.1). The quantum state described by above shape is then $|\chi\rangle = \hat{c}_\varepsilon^\dagger |0\rangle$ with (see eqn. 3.9)

$$\hat{c}_\varepsilon^\dagger = \int \chi(t)\, \hat{a}_\varepsilon^\dagger(t)\, \mathrm{d}t \tag{3.34}$$

$$= \frac{1}{\sqrt{\tau}} \int e^{-\frac{1}{2}\frac{t-t_0}{\tau}} \Theta(t-t_0)\, e^{-i\omega_0 t}\, \hat{a}_\varepsilon^\dagger(t)\, \mathrm{d}t. \tag{3.35}$$

Going back to the second-order correlation function $G_i^{(2)}$ with respect to some initial state $|i\rangle$ before the beam splitter, we exploit the fact that the absolute detection times of the photons t_1 and t_2 are irrelevant, and that we only need to know their difference $\delta t = t_2 - t_1$. We can then integrate over one time variable in eqn. 3.22 and obtain

$$p_i^{(2)}(\delta t)\, \mathrm{d}t = \eta_1 \eta_2\, \mathrm{d}t \int G_i^{(2)}\left(t', t'+\delta t\right) \mathrm{d}t'. \tag{3.36}$$

Since our detectors have a finite time resolution T_D, over which we can assume the second-order correlation function to be constant, we find the absolute probability of detecting a coincidence with a time difference δt within the detector resolution

$$P_i^{(2)}(\delta t) = \eta_1 \eta_2\, T_D \int G_i^{(2)}(t, t+\delta t)\, \mathrm{d}t. \tag{3.37}$$

Introducing the arrival time difference Δt of the photons at the beam splitter and their difference $\Delta\omega$ in frequency, we can now derive the coincidence probabilities for the four

Bell states:

$$P^{(2)}_{\Phi^\pm}(\delta t) = \frac{1}{2}\left(P^{(2)}_{HH}(\delta t) + P^{(2)}_{VV}(\delta t)\right) \tag{3.38}$$

$$P^{(2)}_{\Psi^\pm}(\delta t) = \eta_1\eta_2\frac{T_D}{2\tau}\left[h\,v\,e^{-\frac{|\delta t+\Delta t|}{\tau}} + (1-h)(1-v)\,e^{-\frac{|\delta t-\Delta t|}{\tau}} \mp 2\sqrt{h\,v\,(1-h)(1-v)}\cos(\Delta\omega\,\delta t)\,e^{-\frac{|\delta t|+|\Delta t|}{\tau}}\right] \tag{3.39}$$

with the coincidence probability for the non-entangled state $|HH\rangle$

$$P^{(2)}_{HH}(\delta t) = \eta_1\eta_2\frac{T_D}{2\tau}\left[h^2 e^{-\frac{|\delta t+\Delta t|}{\tau}} + (1-h)^2\,e^{-\frac{|\delta t-\Delta t|}{\tau}} - 2h(1-h)\cos(\Delta\omega\,\delta t)\,e^{-\frac{|\delta t|+|\Delta t|}{\tau}}\right] \tag{3.40}$$

$P^{(2)}_{VV}$ has the same expression as $P^{(2)}_{HH}$ with all transmittances h replaced by v.

The coincidence probability for the three Bell states $|\Phi^\pm\rangle$ and $|\Psi^+\rangle$ is shown in fig. 3.3. We assume identical arrival times of the photons ($\Delta t = 0$) and a difference $\Delta\omega$ in their frequency.

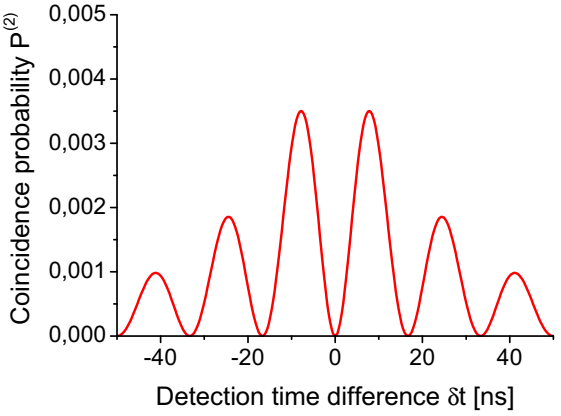

Figure 3.3: Coincidence probability $P^{(2)}$ for the Bell states $|\Phi^\pm\rangle$ and $|\Psi^+\rangle$ ($\eta_1 = \eta_2 = 0.5$, $T_D = 1\,\text{ns}$, $h = v = 0.5$). The photons arrive simultaneously at the beam splitter ($\Delta t = 0$) and have a frequency difference of $\Delta\omega/2\pi = 60\,\text{MHz}$.

The first thing to note is that simultaneous detection events, i.e. $\delta t = 0$, never occur (for identical frequencies, this holds even for any detection time difference δt). This is consistent with the qualitative results from section 2.4, where the photonic wave packets were assumed to have identical shape $\chi(t)$ and carrier frequency ω_0. For an increasing arrival time difference Δt, the photons behave more and more independently as their wave packets no longer overlap. The most prominent thing, however, is the *quantum beat effect* [33], arising when the light frequencies ω_0 of the photons differ. We then have an oscillating behavior of the coincidence probability in the detection time difference δt. This can be understood as follows: once the first photon has been detected, the other photon is in a coherent superposition of the two frequency states, as the frequency of the first photon was not measured by the detectors. The probability amplitudes of the two spatial modes then oscillate with the difference of the frequencies, out of phase with respect to each

other. This yields an oscillating probability of detecting the second photon in one specific output mode, leading to the observed quantum beat of the coincidence probability.

For the state $|\Psi^-\rangle$, the situation is fundamentally different. Here the coincidence probability has a maximum for $\delta t = 0$, i.e. simultaneous detections are more likely than those at different times (see fig. 3.4). This is again in agreement with the qualitative approach. Introducing a difference in the carrier frequencies leads once more to the quantum beat.

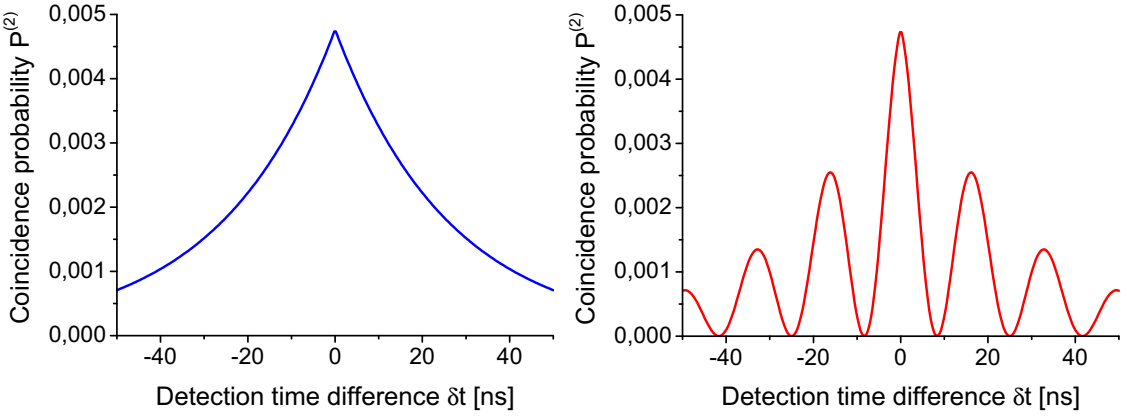

Figure 3.4: Coincidence probability $P^{(2)}$ for the Bell state $|\Psi^-\rangle$ ($\eta_1 = \eta_2 = 0.5$, $T_D = 1\,\text{ns}$, $h = v = 0.5$). The photons arrive simultaneously at the beam splitter ($\Delta t = 0$) and have a frequency difference of (a) $\Delta\omega = 0$ (b) $\Delta\omega/2\pi = 60\,\text{MHz}$.

3.1.5 Entanglement swapping

As was shown in section 2.2, projecting the two photons onto a Bell state implies projecting the pair of atoms onto the very same Bell state. It is therefore imperative to perform the photonic state projection with the greatest possible fidelity, as this is also the fidelity of the entangled atom pair.

After the projection, the atoms are in a state $\hat{\rho}$. Ideally, we have $\hat{\rho} = |\Psi^-\rangle\langle\Psi^-|$, but for a non-perfect Bell measurement, the state is given as a mixture of all four Bell states:

$$\hat{\rho} = \sum_i p_i |i\rangle\langle i| \tag{3.41}$$

with $i \in \{\Phi^\pm, \Psi^\pm\}$. The fidelity of this state with respect to the ideal (pure) state $|\Psi^-\rangle$ is then

$$\begin{aligned} F &= \langle\Psi^-|\hat{\rho}|\Psi^-\rangle && (3.42)\\ &= \sum_i p_i |\langle\Psi^-|i\rangle|^2 && (3.43)\\ &= p_{\Psi^-}. && (3.44) \end{aligned}$$

It follows that the fidelity of the joint atomic state is simply the probability of projecting the two-photon state onto $|\Psi^-\rangle$. This is the figure of merit which we will now derive from

the coincidence probabilities discussed above. The probability of projecting the photons onto $|\Psi^-\rangle$ when detecting a coincidence is given by

$$P^c_{\Psi^-} = \frac{P^{(2)}_{\Psi^-}}{P^{(2)}}, \tag{3.45}$$

where $P^{(2)}_{\Psi^-}$ is the probability of detecting a coincidence caused by the projection onto $|\Psi^-\rangle$ and $P^{(2)}$ is the total probability of detecting a coincidence, including contributions from the other Bell states:

$$P^{(2)} = \sum_i P^{(2)}_i \tag{3.46}$$

The last equation assumes a uniform distribution of all Bell states, which is a valid assumption since we are dealing with unpolarized photons. The fidelity is then found to be

$$F(\delta t) = P^c_{\Psi^-}(\delta t) = \frac{P^{(2)}_{\Psi^-}(\delta t)}{P^{(2)}(\delta t)}. \tag{3.47}$$

For the following calculations, we assume the photonic wave packets to arrive at the beam splitter simultaneously, that means we set $\Delta t = 0$. This is a good approximation, as we will see in section 3.2.1. Another simplification can be made when considering the frequency difference of the two light fields. The emission of the photons stems from the atomic decay in free-space in both traps. Thus the only thing that could induce a frequency difference is Doppler broadening, as the atoms have a finite temperature. A typical value is [16]

$$T_{atom} = 57\,\mu\mathrm{K}, \tag{3.48}$$

giving a Gaussian frequency distribution with the FWHM

$$\Delta f = 220\,\mathrm{kHz}. \tag{3.49}$$

Photons with this frequency difference show a quantum beat with a period of $\approx 4.5\,\mu$s. This is much larger than the lifetime $\tau = 26.23\,$ns of the excited atomic state, which is a measure for the duration of the photons. Hence, it is reasonable to neglect the frequency difference $\Delta\omega$ of the two photons.

With the assumptions, implying indistinguishable photons, the expression for the fidelity is no longer a function of the detection time difference δt but merely of the transmittances h and v:

$$F(h,v) = \frac{1}{2}\frac{2\,h\,v - h - v + 1 + 2\sqrt{h\,v\,(1-h)\,(1-v)}}{2\,h^2 + 2\,v^2 - 3\,h - 3\,v + 2\,h\,v + 2} \tag{3.50}$$

This means that now only the properties of the beam splitter, and not the detection time difference, play a role in obtaining a high fidelity. Intuitively, we expect the highest fidelity, namely $F = 1$, for a perfect beam splitter, i.e. with $h = v = 0.5$. This is confirmed by fig. 3.5, which shows the fidelity as a function of h and v. However, two other cases of interest can be discussed. When setting $h = v = 0$ or $h = v = 1$, we obtain a perfect mirror or complete transmission, respectively. In this case, the photons do not interfere, resulting in one photon in each outgoing mode of the beam splitter, independently of the joint photonic state. Thus only $\frac{1}{4}$ of all coincidences detected are caused by the state

$|\Psi^-\rangle$, hence $F = 0.25$. On the other hand, we obtain a polarizing beam splitter when choosing $h = 0$, $v = 1$ or vice versa. In this case, the Bell states $|\Phi^\pm\rangle$ lead to coincidences in the detectors, while the states $|\Psi^\pm\rangle$ result in the photons leaving the beam splitter in the same mode. Thus a coincidence is never caused by the state $|\Psi^-\rangle$, yielding a fidelity of $F = 0$.

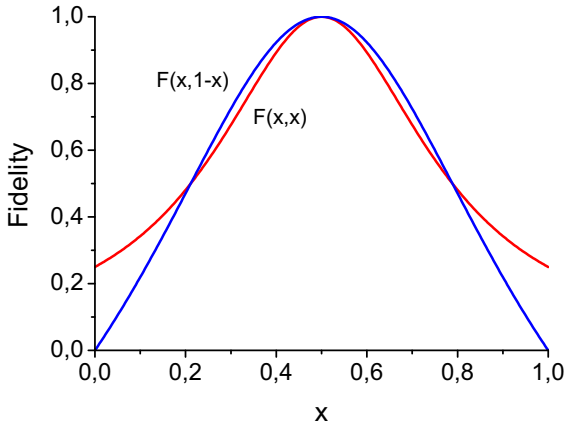

Figure 3.5: Fidelity $F(h, v)$ as a function of the transmission coefficients for identical and overlapped photonic wave packets. The red curve depicts the transition from a perfect mirror ($x = 0$) to perfect transmission ($x = 1$). The blue curve shows the transition from a perfect PBS which reflects horizontal polarization and transmits vertical polarization ($x = 0$) to a PBS fulfilling the opposite ($x = 1$).

In our experiment, the fiber beam splitter has transmission coefficients $h = 0.5221$ and $v = 0.4779$ [30]. From this, the best value for the fidelity which we can achieve is $F = 0.9961$. As the fidelity no longer depends on the detection time difference δt, we can choose the time window in which photons must arrive to be recorded long enough such that the entire wave packets fit in. This yields, of course, the best efficiency, as no photons are rejected.

Summary

In this section, a basic theoretical model to describe two-photon interference was established. The quantization of the light field can be explained in terms of the quantum-mechanical harmonic oscillator. Therefore we use the creation and annihilation operator to describe the light fields entering a beam splitter. The incoming modes are transformed according to the quantum state of the field. As a next step, the detection process was treated quantum-mechanically. Introducing the second-order correlation function, the probability for a coincidence in different output ports of the beam splitter was expressed in terms of the polarization state and temporal shape of the incoming wave packets. For the state $|\Psi^-\rangle$, simultaneous coincidences are more probable than those with a non-zero detection time difference; they are not expected for the other Bell states. For the case of a difference in the carrier frequencies of the photons, a quantum beat in the coincidence probability as a function of the detection time difference can be observed (for all Bell states). As for completing the process of entanglement swapping, it was shown that for ideal conditions (identical wave packets with perfect temporal overlap at the beam splitter and zero frequency difference), the fidelity of the entangled atomic state with respect

to the desired state no longer depends on the detection time difference but only on the quality of the beam splitter. For a perfect beam splitter, the fidelity attains the maximum value of 1. With the beam splitter in our experiment, however, we can achieve a value of 0.9961.

3.2 Experimental realization

In the preceding section, the theorectical framework of two-photon interference was presented. In this part, we describe the way this is realized experimentally. First, an overview of the measurement scheme is given, after which the results will be discussed.

3.2.1 Experimental setup and procedure

As was seen in section 3.1, successful entanglement swapping requires a Bell-state measurement with a high fidelity. One crucial ingredient for a good two-photon interference is the indistinguishability of the photons on the beam splitter. The scale of precision we want to achieve is determined by the duration of the photonic wave packets, given by the decay time $\tau = 26.23\,\text{ns}$ of the excited atomic state. Our detectors are avalanche photodiodes (APDs) with a time resolution of $\approx 1\,\text{ns}$, hence this is the accuracy to which we can synchronize the arrival times of the impinging single-photon wave packets.

The scheme of the experimental procedure is shown in fig. 3.6. Both atom traps are controlled by a single computer and two pattern generators [34]. Once each trap is loaded with a single atom, both atoms are excited with optical laser pulses (cf. section 2.3.1), synchronized by a *start signal distribution* circuit [35].

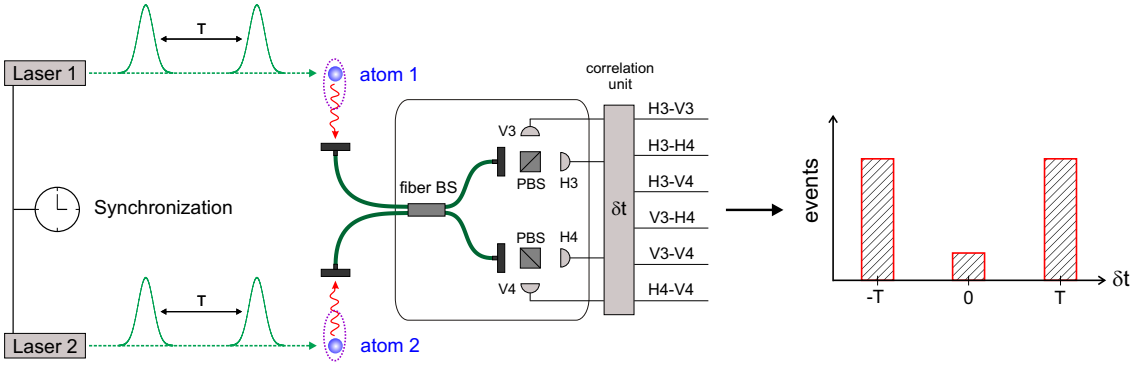

Figure 3.6: Experimental procedure for the observation of two-photon interference. The single atoms in the two traps are synchronously excited by pulses from two independent lasers with a period T. The photons scattered by the atoms are collected and fed into two optical fibers, bringing the photons to interference on the fiber beam splitter. In the outgoing modes of the beam splitter, the polarization states of the photons are analyzed by four single-photon detectors. A correlation unit computes the time difference δt of two consecutive detection events, sorting it into a *cross-correlation* time histogram for each detector pair.

To verify the temporal overlap of the photonic wave packets, a histogram of photon arrival times is measured for each trap. In fig. 3.7, histograms for both traps are shown.

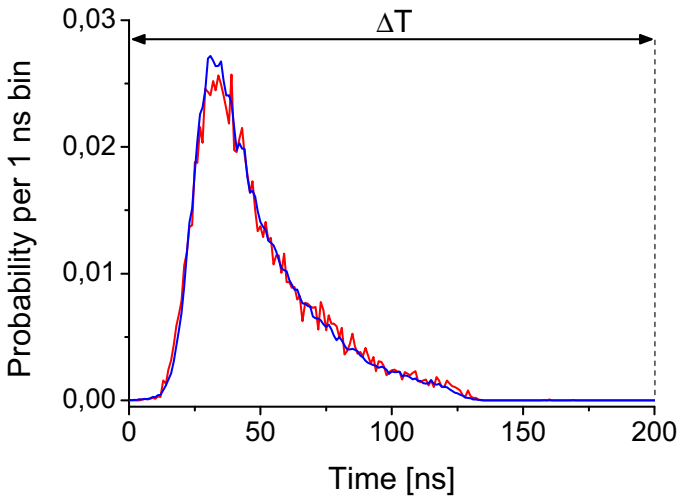

Figure 3.7: Arrival time histogram of photons emitted by one atom in each trap. Each curve corresponds to the photons scattered by one of the atoms. Also shown is the detection time window of length $\Delta T = 200\,\text{ns}$.

3.2.2 Results

We are interested in measuring the quality of the two-photon interference. Given perfect conditions, there are certain pairs of single-photon detections from which we do not expect any simultaneous coincidences. By "simultaneous", we no longer restrict ourselves to the detection time difference $\delta t = 0$, but to coincidences occuring in the same detection time window ΔT. The detection time difference $\delta t = T$ then refers to coincidences in two consecutive detection time windows, where T is the excitation period. In order to evaluate the quality of our two-photon interference, we measure the residual "forbidden" events at $\delta t = 0$ and compare them to the number of coincidences caused by independent, i.e. non-interfering, photons ($\delta t = T$), giving us the *suppression ratio*.

In the following, we will refer to each of the APDs by the polarization they analyze and the outgoing mode of the beam splitter in which they are placed (see fig. 3.1(a)). For example, the detector $H3$ analyzes the horizontal polarization in output mode 3. As was explained in section 2.4, the Bell states $|\Phi^{\pm}\rangle$ cannot be detected by our setup. The states $|\Psi^{\pm}\rangle$, on the other hand, will cause simultaneous coincidences in different detectors. Since the photons are orthogonally polarized for these two Bell states, we should never detect a coincidence between detectors analyzing identical polarizations, namely $H3$-$H4$ and $V3$-$V4$.

We will now consider the probability of an "allowed" coincidence around the detection time difference $\delta t = 0$ for a *given* pair of APDs, i.e. coincidences projecting the joint photonic state onto $|\Psi^{+}\rangle$ or $|\Psi^{-}\rangle$ in a time window of width ΔT. This probability is given by the total collection efficiencies η_1 and η_2 of the two traps. These are the probabilities of detecting a photon after an excitation pulse from the atom in trap 1 and 2, respectively. We find for the probability of an allowed coincidence

$$p_{\delta t=0} = \frac{1}{4} \cdot \frac{1}{2} \cdot \eta_1 \eta_2. \tag{3.51}$$

The factor $\frac{1}{4}$ reflects the probability of the photons being in the analyzed Bell state, while

$\frac{1}{2}$ stems from the fact that there are two possible detector combinations for this state. For example, for the state $|\Psi^-\rangle$, the expected coincidences are in $H3$-$V4$ and $V3$-$H4$. We will now compare this to coincidences of two independent photons. The excitation period in our experiment is $T = 5.34\,\mu$s, which is large compared to the duration of the photonic wave packets. Thus a coincidence in two consecutive time windows is caused by truly independent photons. The probability for detecting a photon from any atom in a given APD after an excitation is

$$p_{ph} = \frac{1}{4}\left(\eta_1 + \eta_2\right), \tag{3.52}$$

hence we find for the probability of a coincidental detection in two APDs in a *given* order:

$$\begin{aligned} p_{\delta t=T} &= p_{ph}^2 && (3.53)\\ &= \frac{1}{16}\left(\eta_1 + \eta_2\right)^2 && (3.54) \end{aligned}$$

We then measure the number of events caused by interfering photons and those caused by independent photons:

$$\frac{N_{\delta t=0}}{N_{\delta t=T}} = \frac{p_{\delta t=0}}{p_{\delta t=T}} = 2\,\frac{\eta_1\eta_2}{\left(\eta_1 + \eta_2\right)^2}. \tag{3.55}$$

For identical efficiencies $\eta_1 = \eta_2$, we obtain

$$\frac{p_{\delta t=0}}{p_{\delta t=T}} = \frac{1}{2}. \tag{3.56}$$

This can also be understood intuitively. For simultaneous detections, both atoms have to contribute a photon at the same time, while for independent coincidences, each atom has the chance to emit twice, namely at time t and at $t + T$. This means that a coincident detection of two photons at these two points in time can originate from two emission processes of the same atom.

Effect of dark counts

We have not yet taken into account the coincidences arising from the dark count events of the single-photon detectors. In principle, a coincidence can arise either from a dark count and a real photon detection or from two dark counts. We will now estimate which suppression ratio can be expected for perfect interference, i.e. when only dark counts can lead to simultaneous detection events in forbidden APD combinations.

The dark count rate of our detectors is d. For a given detection time window of width ΔT, the probability for a dark count in a specific APD is

$$p_{dc} = d\,\Delta T. \tag{3.57}$$

The probability for a coincidence caused by a detected photon and a dark count is then

$$\begin{aligned} p' &= 2\,p_{ph}\,p_{dc} && (3.58)\\ &= \frac{1}{2}\left(\eta_1 + \eta_2\right) d\,\Delta T, && (3.59) \end{aligned}$$

where the factor 2 comes from the fact that it does not matter which APD registered the photon and which one the dark count. Similarly, the probability for a coincidence caused

by two dark counts is

$$p'' = p_{dc}^2 \tag{3.60}$$
$$= (d\,\Delta T)^2\,. \tag{3.61}$$

In general, however, this contribution to the coincidences can be neglected, as $p'' \ll p'$. Using eqn. 3.51, the total probability for a coincidence around $\delta t = 0$ for allowed detector combinations is then

$$p_{\delta t=0}^{(a)} = \frac{1}{8}\,\eta_1\eta_2 + p' + p'', \tag{3.62}$$

while for forbidden coincidences, only the dark counts contribute:

$$p_{\delta t=0}^{(f)} = p' + p''. \tag{3.63}$$

As for coincidences from independent photons, eqn. 3.53 changes accordingly:

$$p_{\delta t=T} = (p_{ph} + p_{dc})^2 \tag{3.64}$$
$$= \left(\frac{1}{4}\,(\eta_1 + \eta_2) + d\,\Delta T\right)^2 \tag{3.65}$$

Cross-correlation histograms

When measuring the two-photon interference, we evaluate the cross-correlation histograms (see fig. 3.8). This means that for each of the six possible detector combinations, the coincidences are sorted into a time histogram according to the detection time difference δt. However, events for combinations pertaining to the same state are added. For example, the cross-correlation histograms of the combinations $H3$-$V4$ and $V3$-$H4$ are combined, as both indicate a projection onto the Bell state $|\Psi^-\rangle$.

From the total number of events in each peak, we can calculate the ratio of simultaneous to independent coincidence detections. The results are shown in tab. 3.1, where we used the mean number of events in the two peaks at $\delta t = T$ and $\delta t = -T$ for the independent coincidences (since the cross-correlation histograms are symmetric about $\delta t = 0$).

	$\|\Psi^-\rangle$	$\|\Psi^+\rangle$	Forbidden
Theory	0.493	0.493	0.016
Measurement	0.477	0.521	0.163

Table 3.1: Ratio of simultaneous to independent coincidence detection events $p_{\delta t=0}/p_{\delta t=T}$. Shown are the theoretical and experimental values for the two Bell states $|\Psi^\pm\rangle$ and for the detector pairs $H3$-$H4$ and $V3$-$V4$, where simultaneous coincidences should by caused by dark counts only (forbidden coincidences). For the calculation of the theoretical values, the collection efficiencies $\eta_1 = 1.24\,‰$ and $\eta_2 = 1.76\,‰$, the dark count rate $d \approx 30\,\mathrm{s}^{-1}$ [36] and the detection window length $\Delta T = 200\,\mathrm{ns}$ were used.

One can see that for the Bell states $|\Psi^\pm\rangle$, the experimental values of the polarization-dependent cross-correlations are in good agreement with the theoretical predictions. The observed small deviations can be ascribed to the statistics of the measurement. For the theoretically suppressed detector combinations $H3$-$H4$ and $V3$-$V4$, however, the suppression ratio was measured to be 0.163, which cannot be explained by statistical fluctuations.

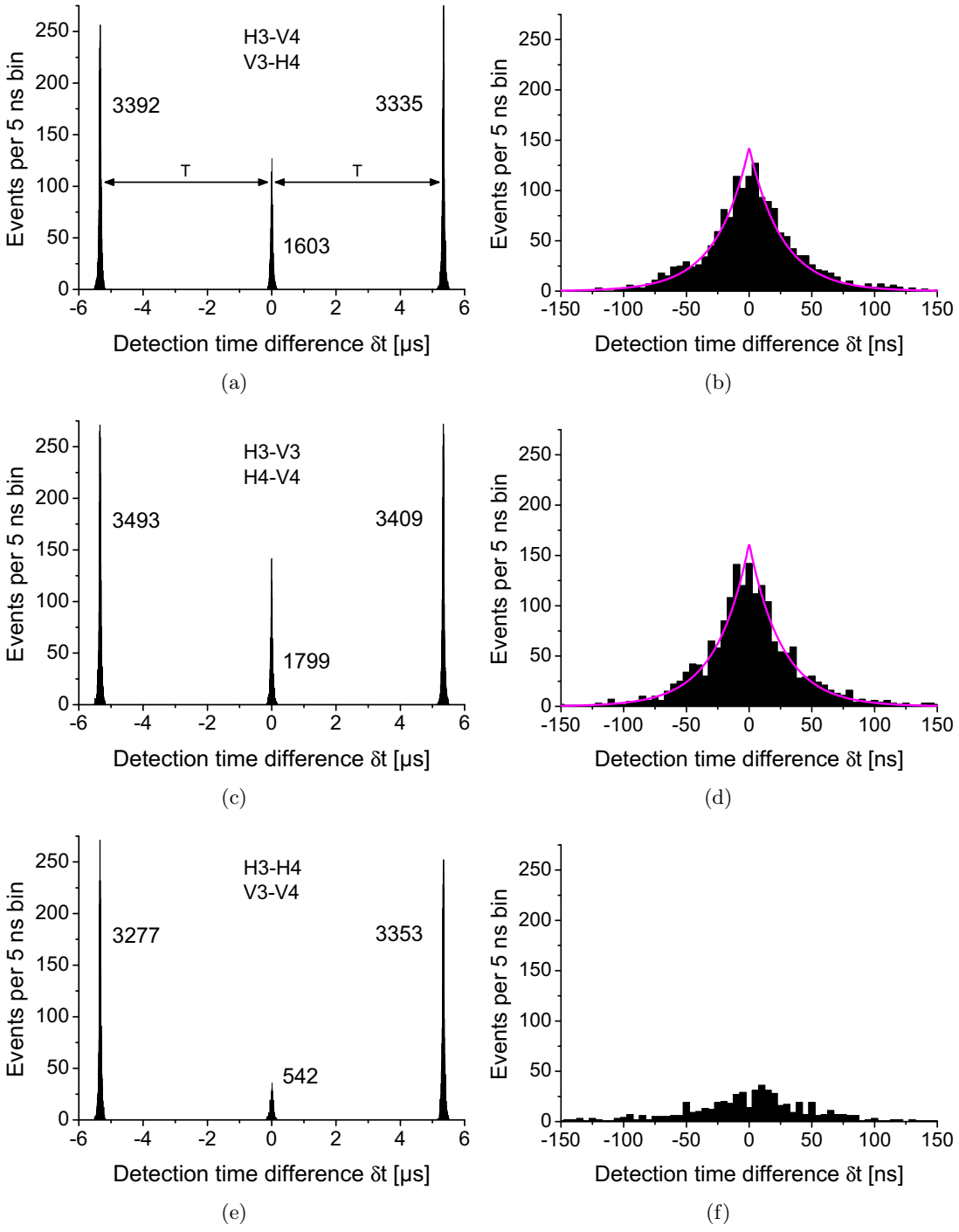

Figure 3.8: Cross-correlation histograms for three pairs of detector combinations. The number next to each peak denotes the total number of events in this peak. (a) (b) APD combination analyzing the Bell state $|\Psi^-\rangle$. The first graph includes the peaks at $\delta t = \pm T$ from the independent coincidences, while the second is a zoom in on the interval $[-150\,\text{ns}, 150\,\text{ns}]$. The magenta curve is a fit of the form $e^{-|\delta t|/\tau}$, showing the validity of eqn. A.7. (c) (d) APD combination analyzing the state $|\Psi^+\rangle$, in analogy to $|\Psi^-\rangle$ (e) (f) APDs analyzing identical polarizations. A zoom in on the theoretically forbidden peak in $[-150\,\text{ns}, 150\,\text{ns}]$ does not yield any pronounced structure compared to the case of the Bell states $|\Psi^\pm\rangle$.

In addition, we consider the *contrast* of the interference, for which a measure is given by the ratio of forbidden simultaneous coincidences to coincidences caused by projections onto the Bell states $|\Psi^{\pm}\rangle$. From fig. 3.8, this ratio is found to be 0.159. This is again much larger than the theoretical value of 0.016 for coincidences caused purely by dark counts, which can be obtained from eqns. 3.62 and 3.63 with the parameters given in tab. 3.1.

This insufficient suppression of forbidden coincidences could, as explained in section 3.1, in principle be caused by a frequency difference of the two photons or by a non-perfect overlap of the wave packets on the beam splitter. As discussed, these effects are well compensated for. The frequency difference caused by Doppler broadening is far too small to induce a quantum beat, while the fiber beam splitter and the synchronized excitation patterns ensure a good spatial and temporal overlap of the photonic wave packets. One point that has not yet been considered is the number of photons in the wave packets. We assumed the atoms to always emit exactly one photon, hence being perfect single-photon sources. Evidently, a wave packet containing more than one photon has a chance of causing a simultaneous coincidence between two detectors, mimicking a successful entanglement swapping event. We will show in the next chapter that the wave packets emitted by the atoms indeed contain more than one photon each when being excited by the laser pulses used in this measurement.

Summary

In this chapter, the idea of quantum interference of two single photons was explained. Having a pair of atoms, each entangled with a photon, the atoms can be entangled by having the photons interfere on a beam splitter. It was shown that for overlapped identical wave packets, only the quality of the beam splitter sets an upper bound for the fidelity of the projected two-photon state with respect to the desired entangled state. In this way, a Bell-state measurement of the joint photonic polarization state can be achieved, projecting the atoms onto an entangled state.

In the experimental section, the synchronization of the atomic excitations was discussed. In order to obtain good interference, the emission times of the photons must not differ by more than $\approx 1\,\mathrm{ns}$. In order to estimate the quality of the two-photon interference, cross-correlation measurements yielded the suppression ratios of coincidences that are not expected in the ideal case. We found that this ratio is significantly larger than can be explained by non-identical / non-overlapped wave packets or coincidences caused by the dark counts of the detectors. One possible reason is the assumption that the photonic wave packets contain exactly 1 photon each. We will see in the next chapter that this is, in fact, not the case.

Chapter 4

Multi-Photon Emission

As was seen in the previous chapter, the principle of two-photon interference requires each of the two atoms to emit exactly one photon. At a first glance, trapped atoms seem perfect candidates to be good single-photon emitters.

This question depends, however, mainly on the relation between the lifetime of the excited atomic state and the duration of the exciting light pulse. Let us consider the case in which the pulse length is large compared to the lifetime of the upper state. While the population of the latter grows during the Rabi cycle, so does the probability to spontaneously decay back to the ground state, emitting a photon. Afterwards, it can be re-excited, assuming the light pulse is not over yet. This then gives a chance of emitting a second photon, after which the atom can again be excited and so on.

For our purpose, the emission of three or more photons can be neglected, but this is not true for two-photon events. In this chapter, we will take a closer look at the conditions under which multi-photon emission can no longer be ignored. The first part will consider a numerical simulation which analyzes the evolution of the quantum-mechanical two-level system given by the atomic ground and excited state under the effect of a driving light field. It will shed light on the question of what kind of excitation pulses are most suited for suppressing unwanted multiple photons. In the second part, a number of experimental pulse forms are discussed and compared to the numerical predictions.

4.1 Numerical considerations

The key to calculating the emission probability of single or multiple photons is to understand the temporal evolution of the atomic two-level system. This evolution is described by the *optical Bloch equations*, which will now be discussed.

4.1.1 Optical Bloch equations for a two-level system

The state of a quantum-mechanical two-level system is in general given by its complex density matrix

$$\rho = \begin{pmatrix} |c_g|^2 & c_{ge} \\ c_{ge}^* & |c_e|^2 \end{pmatrix}. \tag{4.1}$$

The diagonal matrix elements are the probabilities of finding the system in the ground and excited state, respectively, when projecting the system into one these states, e.g. by

making a measurement. The off-diagonal elements quantify the coherence of the system, i.e. they enable to distinguish between coherent superpositions and mixed states.

Another, more convenient way to describe a two-level quantum system is to use the Bloch sphere which was introduced in section 2.1.1. It visualizes not only pure but also mixed states of any two-level system. The state is given by the Bloch vector Π, see fig. 4.1(a). Its Cartesian components u, v, w are defined by the density matrix elements as follows:

$$u = c_{ge} + c_{ge}^* \tag{4.2}$$
$$v = i\left(c_{ge} - c_{ge}^*\right) \tag{4.3}$$
$$w = |c_e|^2 - |c_g|^2 \tag{4.4}$$

The values u, v and w are real numbers in the interval $[-1, 1]$ and are called the dipole moment, dipole current and inversion, respectively. In this picture, the dipole moment and current exhibit the coherence of the state, while the inversion is simply the difference between the populations of the excited and the ground state. For a pure state, the length of Π is always 1, whereas for arbitrary states, we have $|\Pi| \leq 1$. Thus this value is a measure for the purity of a quantum state. For example, a completely mixed state is represented by a point at the origin of the Bloch sphere.

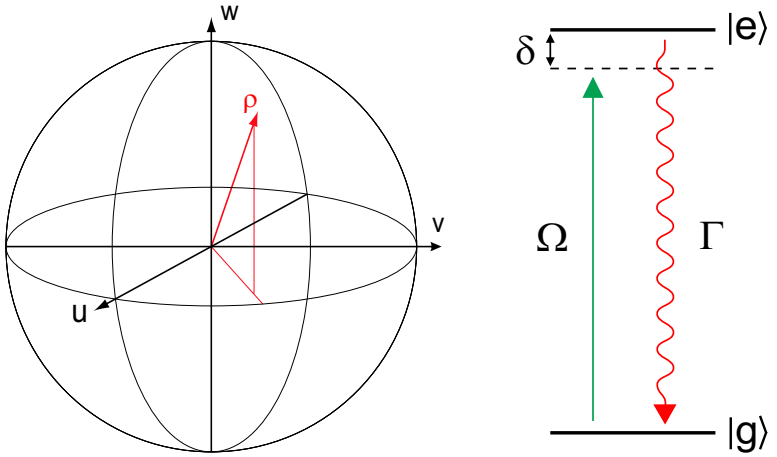

(a) (b)

Figure 4.1: (a) Geometric representation of the Bloch vector in the case of a pure state. For mixed states, the length of the Bloch vector is reduced to a value between 0 and 1. (b) Two-level system with the ground state $|g\rangle$ and excited state $|e\rangle$, coupled by a driving field with Rabi frequency Ω (detuned by δ from resonance). Population of the excited level decays with a rate Γ to the ground state.

Temporal evolution under a driving field

We will now describe the evolution of a given state under the effect of a driving light field. In the semiclassical ansatz, the electromagnetic field of the light is given by a plane wave. Let us assume the following form for the electric field E:

$$\mathbf{E}(t) = \mathbf{E_0}\, f\,(t) \cos\,(\omega t) \tag{4.5}$$

The dimensionless function $f(t)$ denotes the temporal shape of the light pulse, normalized such that its maximum value is 1. The modulus of the electric field E is related to the intensity I of the light beam by

$$I = \frac{1}{2} c \varepsilon_0 E^2 \tag{4.6}$$

when in vacuum (which is the case for our experiment).

In the dipole approximation [31], the field couples to the dipole matrix element $\boldsymbol{\mu}_{ge} = \langle e | \hat{\boldsymbol{\mu}} | g \rangle$. Defining the time-dependent Rabi frequency $\Omega(t) = \boldsymbol{\mu} \cdot \mathbf{E_0} f(t)/\hbar$, the detuning $\delta = \omega - \omega_0$ (with resonance frequency ω_0) and the decay rate $\Gamma = \frac{1}{\tau}$ (with excited level lifetime $\tau = 26.23\,\text{ns}$), the optical Bloch equations can be written as [31]

$$\dot{u} = \delta v - \frac{\Gamma}{2} u \tag{4.7}$$

$$\dot{v} = -\delta u + \Omega(t)\, w - \frac{\Gamma}{2} v \tag{4.8}$$

$$\dot{w} = -\Omega(t)\, v - \Gamma (w + 1) \tag{4.9}$$

for a given initial state $\Pi(0)$. Fig. 4.1(b) shows a schematic of this evolution. In general, this set of differential equations can only be solved numerically for a given shape $f(t)$ of the excitation pulse. We are particularly interested in two pulse forms:

a) a simple rectangular pulse, defined by

$$f(t) = \begin{cases} 1, & |t - t_0| \leq \Delta t/2 \\ 0, & |t - t_0| > \Delta t/2 \end{cases} \tag{4.10}$$

b) a Gaussian pulse, defined by

$$f(t) = e^{-4 \ln 2 \left(\frac{t - t_0}{\Delta t}\right)^2} \tag{4.11}$$

Δt and t_0 denote the full width at half maximum (FWHM) and the center of the pulse, respectively. The Rabi frequency then takes the form $\Omega(t) = \Omega_0 f(t)$.

In our first consideration, we will investigate the evolution of the two-level system under a π-*pulse*, i.e. a pulse fulfilling the condition

$$A := \int_{-\infty}^{+\infty} \Omega(t)\, \mathrm{d}t = \pi, \tag{4.12}$$

where A is the *pulse area*. This means that, in absence of spontaneous decay, the system undergoes half a Rabi cycle. Starting from the ground state, the system is entirely transferred to the excited state, and vice versa. It is our goal to implement pulse areas as close to π as possible, since this gives us the best excitation efficiency. Using eqn. 4.12, we can determine the peak Rabi frequency Ω_0 as a function of the FWHM Δt to be

$$\Omega_{0,rect} = \frac{\pi}{\Delta t} \tag{4.13}$$

for a rectangular pulse and

$$\Omega_{0,Gauss} = \frac{\sqrt{4\pi \ln 2}}{\Delta t} \tag{4.14}$$

for a Gaussian pulse. Figs. 4.2(a) and 4.2(b) show the temporal evolution of the system for a rectangular and a Gaussian excitation pulse. It can be seen, since the duration of the exciting pulse is on the order of the upper state lifetime, that spontaneous decay prevents the system from reaching the upper state. For shorter pulses, more population can be transferred to the excited state. The figures also show the system reaching a lower population inversion for a Gaussian pulse, as the wings of the Gaussian shape make a contribution to the excitation which lies outside the FWHM Δt. This makes the pulse effectively longer, resulting in a lower excitation probability (despite the pulse area being the same as for the rectangular shape).

We are also interested in the behavior of the system if the light field is detuned by an amount δ from the atomic resonance. The system then does not attain the maximum population inversion, but reaches an intermediate superposition of ground and excited state. Since this happens in a shorter time than for the resonant case, the atom is partly de-excited before the pulse is over. Altogether, a detuned π-pulse leads to a smaller peak population inversion than for the resonant case (see fig. 4.2(c)).

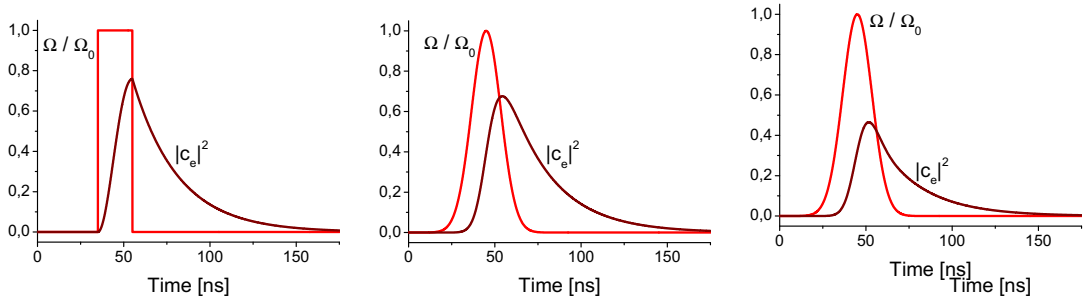

Figure 4.2: Evolution of the upper level population of a two-level system which is initially in the ground state under a π-pulse of (a) rectangular shape (b) Gaussian shape with zero detuning (c) Gaussian shape with a detuning of $\delta/2\pi = 15\,\mathrm{MHz}$. All pulses have a FWHM of $\Delta t = 20\,\mathrm{ns}$.

4.1.2 Probability for emitting multiple photons

Now that we have a tool at hand to describe the effect of a light field on an atomic dipole, we will consider the question of how many photons the atom emits during the excitation process. We will approach this problem using a *quantum jump* picture [37]. The photon detectors play the role of a measuring device, continuously determining whether the atom emitted a photon. This means that as long as no photon is detected, the atom undergoes a *coherent* evolution, governed only by the driving field. However, a population of the excited atomic state gives rise to a non-vanishing probability of emitting a photon in a given (infinitesimal) time interval. If a photon is detected, the atomic state is projected onto the ground state, i.e. the atom decays instantly, "jumping" to the ground state. It then continues its coherent evolution, assuming the light pulse is not over. This process, illustrated in fig. 4.3, can be repeated many times, depending on the duration of the light pulse. This picture explains qualitatively why a long pulse will cause the atom to emit more than one photon.

Before considering the emission of one or more photons, we will derive an expression

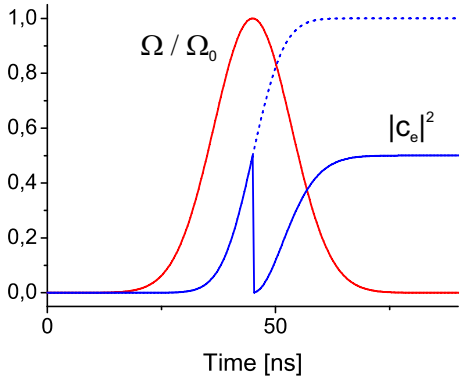

Figure 4.3: The effect of spontaneous decay in the quantum jump picture. The atom undergoes a coherent evolution, governed solely by the driving light field. The probability for a decay to the ground state rises proportionally to the upper state population. At some point in time, the atom decays instantly, emitting a photon and restarting its coherent evolution from the ground state.

for the probability $p_0(t)$ of *not* emitting a photon up to the time t. Let us assume a time interval that is split into two smaller intervals. Not finding a photon in the entire interval means not finding a photon in each of the sub-intervals. It follows that the probability of not finding a photon in the entire interval is simply the product of the probabilities for the sub-intervals. Hence, assuming that $p_0(t)$ is given for some t, the probability $p_0(t+\mathrm{d}t)$ of *still* not having emitted a photon after a time step $\mathrm{d}t$ is found to be

$$p_0(t+\mathrm{d}t) = p_0(t) + \mathrm{d}p_0 = p_0(t)(1 - p\,\mathrm{d}t), \tag{4.15}$$

where $p\,\mathrm{d}t$ is the probability of emitting a photon within the time $[t, t+\mathrm{d}t]$:

$$p\,\mathrm{d}t = \Gamma |c_e(t)|^2 \,\mathrm{d}t, \tag{4.16}$$

where the upper state population $|c_e(t)|^2$ is related to the inversion via $|c_e|^2 = \frac{w+1}{2}$ (see eqn. 4.4). Combining these two expressions leads us to the following differential equation for p_0:

$$\dot{p_0}(t) = -\Gamma |c_e(t)|^2 p_0(t) \tag{4.17}$$

A formal solution is given by integration:

$$p_0(t) = \exp\left(-\int_{-\infty}^{t} \Gamma \left|c_e(t')\right|^2 \mathrm{d}t'\right) \tag{4.18}$$

Therefore by solving the optical Bloch equations, we can compute $p_0(t)$ by essentially integrating over the upper state population. For all further considerations, we will extend p_0 to be the probability of not emitting a photon between the times t_1 and t_2, thus obtaining

$$p_0(t_1, t_2) = \exp\left(-\int_{t_1}^{t_2} \Gamma \left|c_e(t')\right|^2 \mathrm{d}t'\right). \tag{4.19}$$

In order to investigate the probability of the atom emitting one or more photons, we consider the case in which no photon is emitted up to a time t, followed by an emission in

the interval $[t, t + \mathrm{d}t]$, after which no further photon is observed. The probability for this is

$$\begin{aligned} \mathrm{d}p_1 &= p_0(-\infty, t)\, p\, \mathrm{d}t\, p_0(t, \infty) && (4.20) \\ &= p_0(-\infty, t)\, \Gamma \left|c_e(t)\right|^2 p_0(t, \infty)\, \mathrm{d}t, && (4.21) \end{aligned}$$

leading us to an expression for the probability of emitting exactly one photon up to the time t and no more afterwards:

$$p_1(t) = \int_{-\infty}^{t} p_0\left(-\infty, t'\right) \Gamma \left|c_e\left(t'\right)\right|^2 p_0\left(t', \infty\right) \mathrm{d}t' \tag{4.22}$$

For calculating $p_0(t, \infty)$, it is important to note that after the emission of a photon, the system is in its ground state at time t and restarts its coherent evolution from there. For $p_0(-\infty, t)$, the system can be in any initial state at time $t = -\infty$. Via eqns. 4.18 and 4.22, we now have the probability of emitting multiple, i.e. two or more, photons up to the time t:

$$p_m(t) = 1 - p_0(t) - p_1(t) \tag{4.23}$$

Computing $p_1(t)$ and thus $p_m(t)$ is numerically expensive, which means long computing times are to be expected from solving above integrals. A brief insight into this problem and how it can be solved is given in appendix A.2.

Having now the means to describe both the evolution of the atomic state and the emission probabilities for one and for multiple photons, we will examine the light scattering behavior of the atom under a variation of different properties of the excitation pulse, namely the duration, the pulse area and the detuning. The peak Rabi frequency Ω_0 does not play an independent role in this, as it is always given by the duration Δt and pulse area A (see eqn. 4.12).

To obtain a first insight, we consider the temporal evolution of the excited atomic state and the emission probabilities during the excitation process. We apply a π-pulse of 20 ns length with a rectangular and a Gaussian shape, respectively. The temporal evolution of p_1 and $p_1 + p_m$ is shown in fig. 4.4. It can be seen that the probability of emitting at least one photon rises continuously, even after the end of the excitation pulse. This is because the lifetime of the atom exceeds the pulse duration, i.e. the upper state is still at least partially populated after the pulse. The longer we wait, the more probable it is for the atom to decay and emit a photon. As the pulse area is $A = \pi$, we will observe a photon with certainty, although, strictly speaking, only after an infinite time. The probability for finding more than one photon, on the other hand, saturates at the end of the pulse. This can be intuitively understood, since only if the atom decays during the pulse, it can be re-excited such that it can emit another photon. When comparing π-pulses of 20 ns duration with different shapes, it is interesting to note that the Gaussian pulse results in a multi-photon probability of $p_{m,Gauss} = 15.19\,\%$, which is larger than $p_{m,rect} = 9.23\,\%$ for the rectangular shape. This is, similar to the peak population inversion mentioned above, due to the wings of the Gaussian shape, which make the pulse effectively longer, thus increasing the probability of re-exciting the atom after the first photon emission. Having examined these two particular cases, we will now vary the parameters Δt, A and δ and see how this affects the emission probabilities.

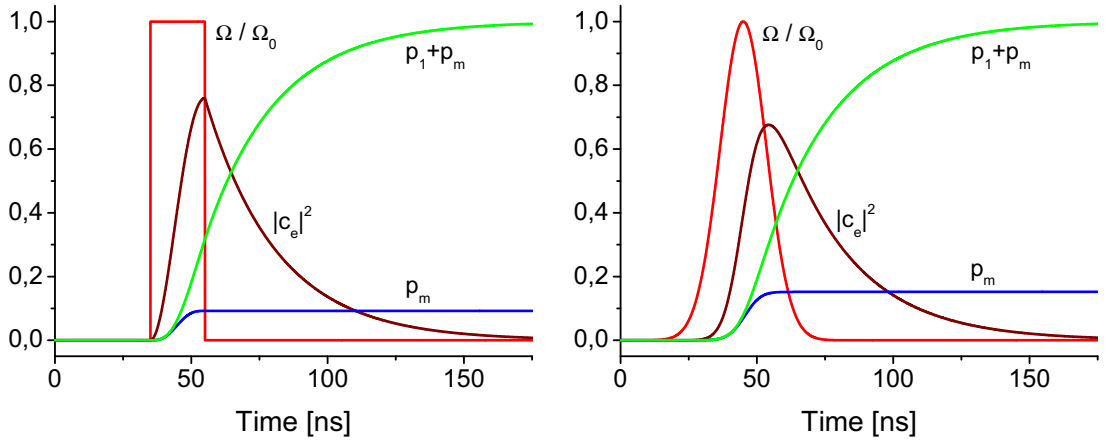

Figure 4.4: Evolution of the upper state population $|c_e|^2$ and the probabilities for emitting at least one photon ($p_1 + p_m$) and more than one photon (p_m). The π-pulses have a FWHM of $\Delta t = 20\,\text{ns}$ and (a) rectangular (b) Gaussian shape.

Multi-photon emission for varying pulse parameters

As mentioned before, shorter pulses should reduce the emission of multiple photons, which means it is favorable to fulfill the condition $\Delta t \ll \tau$. This becomes obvious when looking at fig. 4.5, where the probability for emitting more than one photon is plotted as a function of the FWHM Δt of the excitation pulse. The numerical solution of equation 4.23 is computed for 100 values of $\Delta t \in [1\,\text{ns}, 20\,\text{ns}]$. We can afford to use such a large number of points due to the algorithm sketched in appendix A.2. As was said earlier, the Gaussian pulse form results in a consistently larger probability for a multi-photon emission, independent of the particular pulse width. The interesting part is the regime of pulse durations below 5 ns, which are still experimentally feasible and lead to emission probabilities of more than one photon of $p_m < 3.3\,\%$. However, for a very good suppression of multi-photon events, say $p_m < 1\,\%$, pulse widths below 1.5 ns are needed.

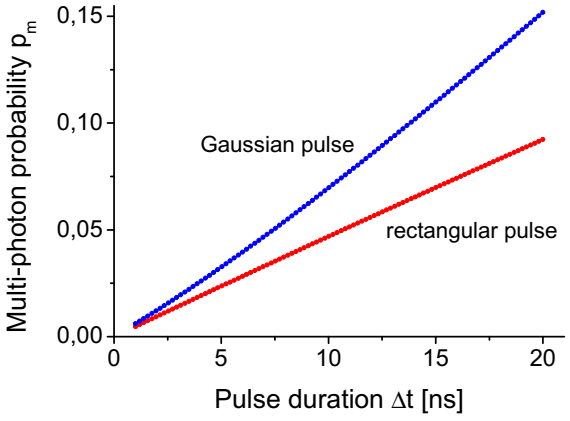

Figure 4.5: Emission probability for more than one photon for π-pulses with variable width Δt. Note that the probability of finding *at least* one photon is always 1.

The next parameter to be varied is the pulse area A. So far, we have considered π-pulses because they yield the highest probability of causing a photon emission. However, it is promising to reduce the pulse area below π. This reduces the emission events as a whole, but in particular the multi-photon events are reduced further than the one-photon events. Because, for a single photon, the atom must be excited and then decay, it is clear that when reducing the pulse area, the probability for this event becomes smaller. The probability then of emitting a second photon, which is directly related to the ratio of single-photon to multi-photon events, is also reduced, since it depeends on the pulse area in the same way. This makes multi-photon events much more unlikely for smaller pulse areas. This behavior is confirmed by fig. 4.6(a), where the calculated probabilities for an emission of at least one and more than one photon are plotted for different pulse areas. For A significantly smaller than π, both values drop by several orders of magnitude, but the multi-photon probability declines more steeply. The ratio of single-photon to multi-photon events rises by more than 4 orders of magnitude for $A = 0.04\,\pi$, although this leads to a total photon probability of merely 2 %. Thus we have a trade-off between a small multi-photon probability and a good excitation probability. A decent pulse area might be $A = 0.4\,\pi$, giving a single-photon to multi-photon emission ratio of 97:1 (compared to 5.6:1 for a π-pulse) while still maintaining an overall emission probability of 86 %.

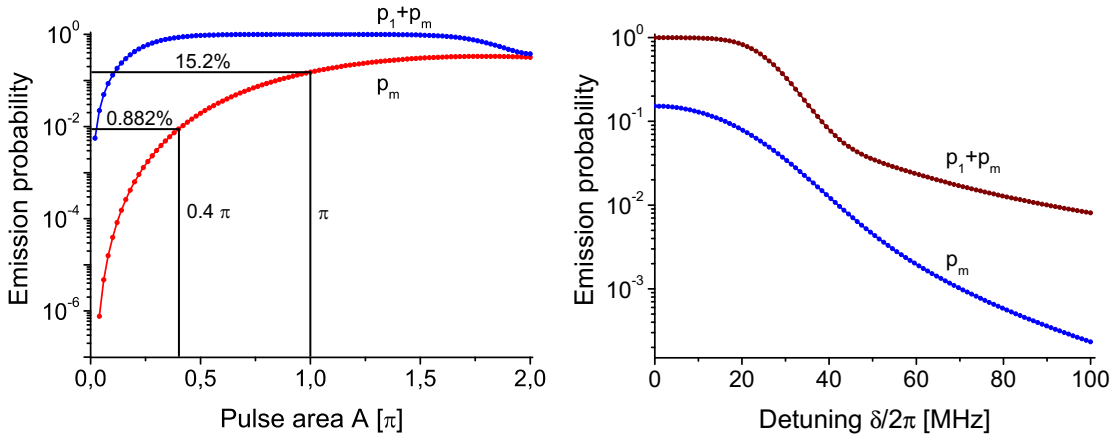

Figure 4.6: Emission probabilities for a Gaussian pulse with duration $\Delta t = 20\,\text{ns}$. (a) Variable pulse area between 0 and 2π (b) Variable detuning from the atomic resonance

Finally, we are interested in the effect of the detuning δ of the excitation light field from the atomic resonance. Again, we use π-pulses of 20 ns duration and Gaussian shape and vary the detuning in a range $\delta/2\pi \in [0, 100\,\text{MHz}]$ (see fig. 4.6(b)). For comparison, the peak Rabi frequency for these parameters is $\Omega_0/2\pi = 23.5\,\text{MHz}$. The most prominent effect is that the ratio of probabilities for single and multiple photons is roughly constant (about 1 order of magnitude). Thus choosing a detuning $\delta \neq 0$ will not give us any significant improvement over the resonant case. On the contrary, it degrades the emission probability, by a factor, for example, of 124 for $\delta/2\pi = 100\,\text{MHz}$. As explained in section 4.1.1, this is due to the multiple Rabi oscillations induced by the light pulse for sufficient detuning. Therefore the atom not only reaches a smaller population inversion but is also partly de-excited before it can emit a photon.

Summary

In this section, the notion of multi-photon emission from an atom under a pulsed laser excitation was investigated theoretically. The behavior of the atomic dipole under a driving light field is described by the optical Bloch equations. The probabilities of observing one or several photons is then given by the coherent population inversion. In order to suppress the unwanted emission of more than one photon, the duration of the pulse as well as the pulse area may be reduced. The first has experimental limits, as achieving pulse widths below 5 ns is not easily done, whereas the latter reduces the overall probability of emitting a photon at all. Still, these two parameters provide means to improve the ratio of single-photon to multi-photon events without degrading the excitation probability too much. In contrast, the detuning of the light field from the atomic resonance does not improve the single-photon to multi-photon emission ratio.

However, these calculations were done under the assumption that the atom exhibits a simple two-level structure. This is, of course, not true for real atoms, as those used in our experiment. As will be seen, these multi-level effects play an important rule in the matter of multi-photon emission and will briefly be discussed in section 4.3.

4.2 Experimental results

The numerical considerations in the previous section gave us a good estimate on the emission probabilities that can be expected for one or multiple photons with different types of exciting light pulses. The next step is to look at what can be done experimentally to achieve a low probability of multi-photon emission. We will first introduce the way in which this is measured and then compare it to the numerical simulation.

4.2.1 Measuring the multi-photon probability

As explained in section 3.1.4, we record the arrival times of the spontaneously emitted photons in a time histogram. To deduce the fraction of multi-photon events, we use a Hanbury-Brown-Twiss (HBT) setup [38]. This is a non-polarizing beam splitter behind which two single-photon detectors are placed. The incoming light field is split and directed onto the detectors. The point in time of a detection is then fed into a correlation unit which calculates the time difference δt of two consecutive detection events and sorts this into a histogram. This time difference histogram is then the autocorrelation function of the light field, being a direct measure for the $g^{(2)}$ function [25]. Fig. 4.7 shows a schematic of the setup and a sketch of the autocorrelation function for a pulsed photon source. Pulses containing more than one photon have a chance of causing simultaneous clicks in the detectors (i.e. events in the same detection time window), giving rise to a peak in the photon detection histogram at the time difference $\delta t = 0$. The number of these events must be compared to events caused by consecutive excitation pulses. For a clear distinction between the peaks, the excitation period T (5.34 μs in our case) must be large compared to the lifetime of the excited atomic state (26.23 ns).

We want to use the autocorrelation histograms to deduce the ratio of single-photon to multi-photon events. We will neglect the probability of emitting more than two photons, as it is much smaller than the probabilities for exactly one or two photons [37]. The probability for detecting two photons from the atom after an excitation (where the order

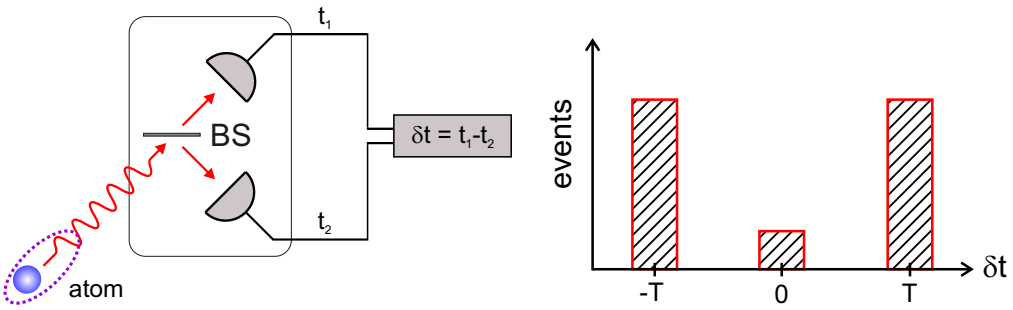

(a) (b)

Figure 4.7: (a) Schematic of measuring the autocorrelation function of the light emitted by an atom in the Hanbury-Brown-Twiss configuration. Light pulses containing multiple photons have a chance of triggering simultaneous clicks in the single-photon detectors. (b) Sketch of a histogram of the arrival time difference δt for a light source emitting pulses with excitation period T

in which the detectors click does not play a role) is

$$p_{\delta t=0} = \frac{1}{2}\,\eta^2\,p_2, \tag{4.24}$$

with η being the overall collection efficiency of the optics and p_2 the two-photon emission probability. The factor $\frac{1}{2}$ stems from the fact that two photons hit different detectors only in 50 % of all cases. On the other hand, the probability to detect two independent photons from consecutive excitations *in a given order* (i.e. one specific detector clicks first) is

$$p_{\delta t=T} = \left(\frac{1}{2}\,\eta\,p_1\right)^2. \tag{4.25}$$

We directly measure the number of simultaneous and independent events $N_{\delta t=0}$ and $N_{\delta t=T}$, respectively, and calculate the ratio

$$\frac{N_{\delta t=0}}{N_{\delta t=T}} = \frac{p_{\delta t=0}}{p_{\delta t=T}} = \frac{2\,p_2}{p_1^2}. \tag{4.26}$$

For short π-pulses we can set $p_1 \approx 1$ and obtain for the ratio of multi-photon to single-photon emission

$$\frac{p_m}{p_1} \approx \frac{p_2}{p_1} \approx \frac{1}{2}\,\frac{N_{\delta t=0}}{N_{\delta t=T}}. \tag{4.27}$$

To improve our statistics, we use the mean number of events at $\delta t = T$ and $\delta t = -T$, which we can do since the autocorrelation function is symmetric about $\delta t = 0$. An important point to note is that in our setup, we use two detectors in each outgoing mode of the beam splitter, since we perform polarization analyses for the two-photon interference (cf. section 3.1). Thus we need to sum up the number of detection events in each outgoing mode, as we are not interested in the polarization states of the photons.

Experimental pulse forms

Since we have now the tools to estimate the number of multi-photon emissions from the atom, we will try to minimize these by using different forms of the excitation pulse. Four

different forms are investigated experimentally. The first is a standard Gaussian pulse with a FWHM of $\Delta t = 26.3\,\text{ns}$ of the Rabi frequency, followed by two rectangular ($\Delta t = 15.2\,\text{ns}$ and $\Delta t = 6.05\,\text{ns}$) and a sawtooth ($\Delta t = 4.45\,\text{ns}$) shaped pulse. The Gaussian pulse is shown in fig. 4.8. Here we were able to use an appropriate fit to determine the FWHM. For the other pulse forms, no value tables were available; in order to obtain a parameterized function for the pulses, piecewise analytical funtions were used to describe the pulse form $f(t)$. This can be seen in fig. 4.9 and is needed later on for the comparison of the experimental values to the numerical simulation. The Gaussian pulse is formed using only an acousto-optic modulator (AOM) with a bandwidth of 25 MHz. For pulses significantly shorter than 20 ns, an electro-optic modulator (EOM) with a bandwidth of 200 MHz is placed before the AOM stage. For example, the EOM forms the steep rising slope of the sawtooth shaped pulse, while the AOM defines the almost linear decay.

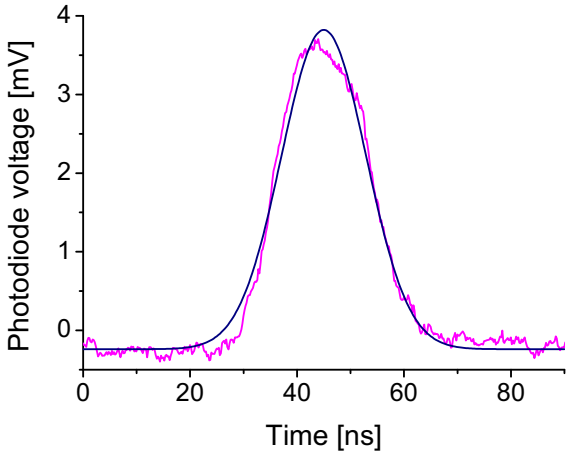

Figure 4.8: Temporal shape of the standard Gaussian excitation pulse, measured with a fast photodiode. A Gaussian fit (blue curve) yields a FWHM of the light intensity of $18.61 \pm 0.13\,\text{ns}$. Intensity and Rabi frequency are related via $I \propto \Omega^2$, thus giving a FWHM of the Rabi frequency of $\Delta t = 26.3\,\text{ns}$.

Results

From the measured histograms, we can now calculate the ratio $N_{\delta t=0}/N_{\delta t=T}$ of simultaneous to independent events, which gives us a good estimate of the ratio p_m/p_1, according to eqn. 4.27. The autocorrelation histograms are shown in fig. 4.9, together with a the temporal shapes of the excitation pulses. As expected, the long Gaussian pulse produces the highest probability for multiple photons with a multi-photon to single-photon emission ratio of $p_m/p_1 = 6.08\,\%$. The long rectangular pulse shows an improvement with $p_m/p_1 = 4.33\,\%$, but reducing its duration makes the ratio worse again ($p_m/p_1 = 5.07\,\%$). This is due to the bad switching off property of the EOM. In contrast, the sawtooth shaped pulse shows a considerably improved emission ratio compared to the Gaussian pulse with $p_m/p_1 = 3.46\,\%$.

A way to further improve the multi-photon to single-photon emission ratio is to discard photons which are emitted by the atom while the excitation light is still present. Counting only photons which originate from the exponential decay of the upper atomic state after the light pulse, it should be possible, at least in theory, to completely suppress multi-photon

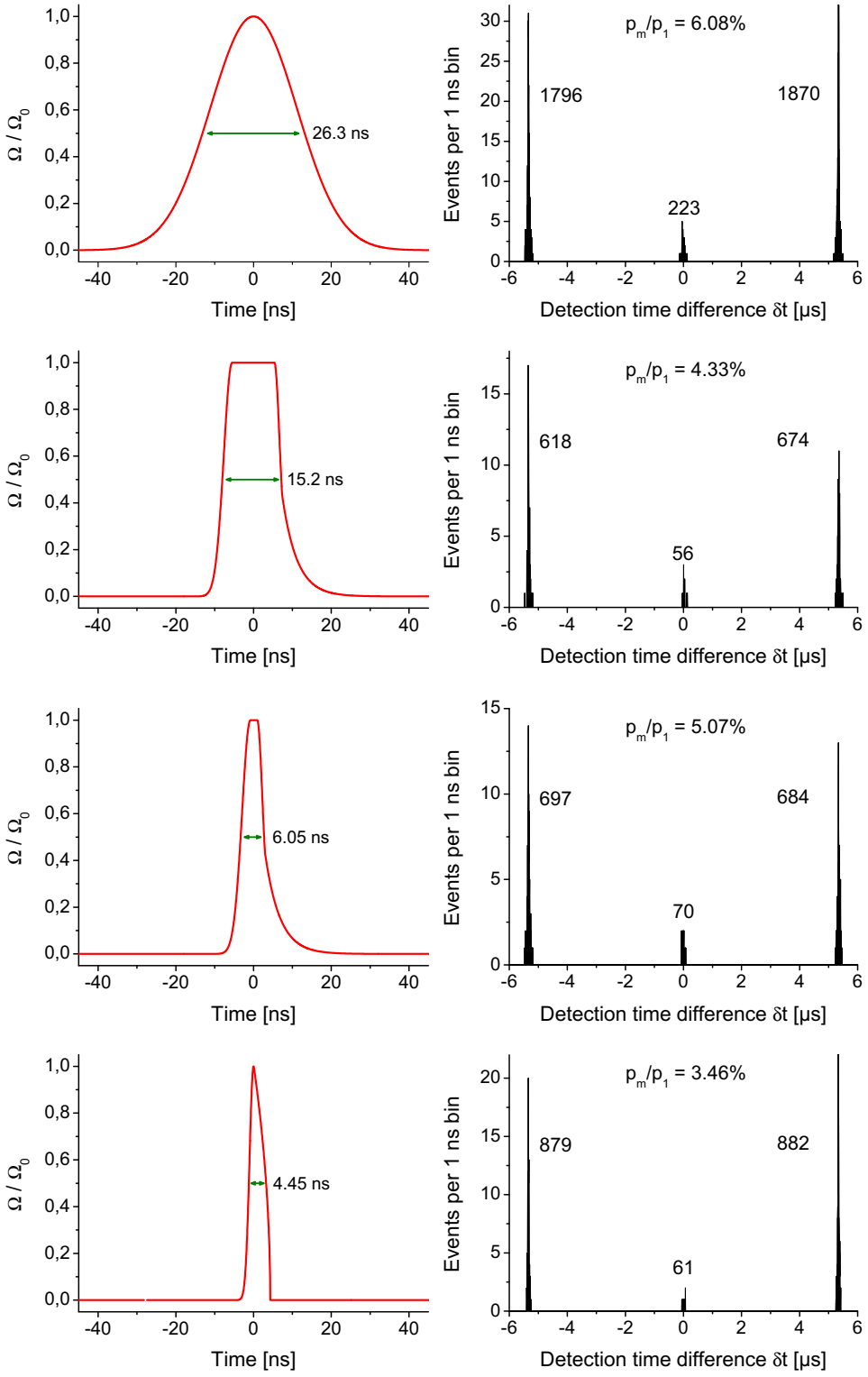

Figure 4.9: Experimentally measured autocorrelation histograms. Each histogram was obtained for a pulse of which the parameterized form can be seen in the adjacent graph. The numbers next to the peaks denote the total number of detection events in the respective peak. From top to bottom, the standard Gaussian, the long and short rectangular and the sawtooth pulse are shown.

events. This is because after the emission of a photon, the atom decays to the ground state, from where it cannot be re-excited since there is no longer a driving field present. The drawback of this method is obviously the loss in the total emission probability. However, this selection of photons was done for the sawtooth pulse, to be seen in fig. 4.10. It yielded a multi-photon to single-photon ratio of $p_m/p_1 = 1.64\,\%$, an improvement by more than a factor of 2 compared to accepting all photons. From the arrival time histogram, one can infer that the total emission efficiency is reduced by 22 %.

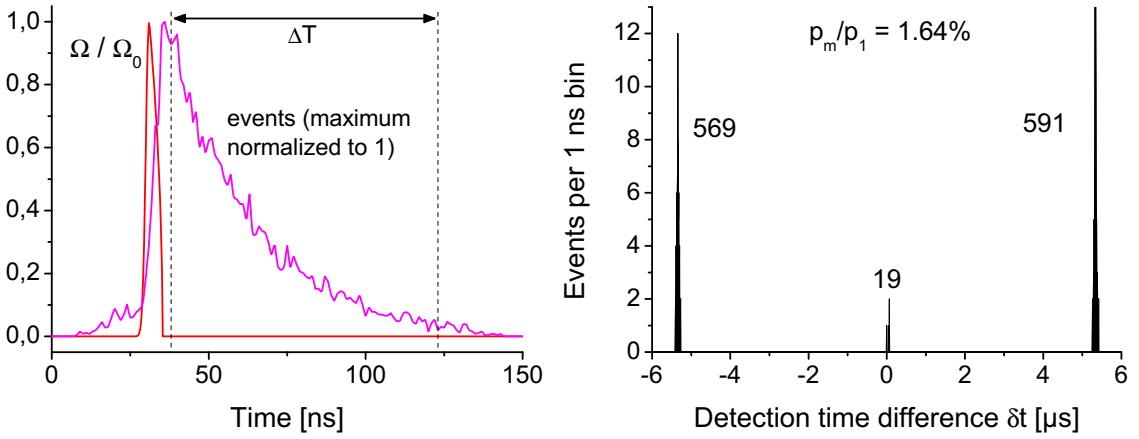

(a) (b)

Figure 4.10: (a) Arrival time histogram for the excitation with a sawtooth pulse. The cropped time window [38 ns, 123 ns] in which photons are accepted begins at the end of the excitation pulse. All photons lying in this window then originate solely from the exponential decay of the atomic excited state after the pulse, in principle suppressing any multi-photon emission. (b) Autocorrelation histogram yielding the ratio $p_m/p_1 = 1.64\,\%$

Effect of dark counts

We have not yet taken into account the coincidences arising from the dark count events of the single-photon detectors. The following calculations are similar to those presented in section 3.2.2 concerning the quality of the two-photon interference. We will now estimate which multi-photon to single-photon emission ratio can be expected for a perfect single-photon source, so essentially when only dark counts of the detectors are present.

The dark count rate of our detectors is again denoted by d. As the setup is designed to measure two-photon interference with polarization analyses in the outgoing modes (see previous chapter), we use two detectors in each of the outgoing spatial modes of the beam splitter. For a given time window of length ΔT, in which we expect a photon from the excitation of the atom, the probability for a dark count in one APD is

$$p_{dc} = d\,\Delta T, \tag{4.28}$$

whereas the probability for a real photon is

$$p_{ph} = \eta, \tag{4.29}$$

with η being the overall detection efficiency. The probability for a coincidence caused by a photon and a dark count is then given by

$$p' = \frac{1}{2} p_{ph} \cdot 4\, p_{dc} \tag{4.30}$$
$$= 2\,\eta\, d\, \Delta T. \tag{4.31}$$

The factor $\frac{1}{2}$ comes from the fact that when detecting the photon in one spatial output mode of the beam splitter, the dark count must occur in the other output mode in order to cause a coincidence, which happens only in 50 % of all dark count events. The factor 4 stems from the fact that four APDs contribute to the dark count events. Similarly, we find for the probability for a coincidence caused by two dark counts

$$p'' = 4\, p_{dc} \cdot 2\, p_{dc} \tag{4.32}$$
$$= 8\,(d\,\Delta T)^2\,. \tag{4.33}$$

As for the two-photon interference, p'' can be neglected compared to p' in most cases. The multi-photon to single-photon ratio given by eqn. 4.27 is then

$$\frac{p_m}{p_1} = \frac{1}{2}\frac{N_{\delta t=0}}{N_{\delta t=T}} = \frac{1}{2}\frac{N_{exc}\,(p' + p'')}{N_{\delta t=T}}, \tag{4.34}$$

where N_{exc} is the number of excitations during a measurement.

We will evaluate this quantity for the sawtooth shaped pulse in combination with the cropped detection time window. Our avalanche photodiodes have a dark count rate of $d \approx 30\,\mathrm{s}^{-1}$ [36], the width of the detection window is $\Delta T = 85\,\mathrm{ns}$, the collection efficiency is $\eta = 0.99\,‰$ and the number of excitations is $N_{exc} = 3142051780$. From these values we deduce

$$\frac{p_m}{p_1} = 1.4\,\% \tag{4.35}$$

for an ideal single-photon source, however, with imperfect detectors. We find that this value is in good agreement with the experimentally observed value of $p_m/p_1 = 1.64\,\%$, concluding that the remaining multi-photon emission probability is negligible.

4.2.2 Comparison to the numerical simulation

As the next step, we calculate the probabilities for single- and multi-photon emissions from experimentally chosen excitation pulses in order to compare theory and experiment. For the use of above pulse forms, it is necessary to know the peak Rabi frequencies Ω_0 of the pulses. One possibility to determine these is to measure the power and beam radius of the excitation light at the position of the atom. However, these data are not always available and we therefore resort to the histograms of the arrival times of the spontaneously scattered photons. From these we can deduce the temporal evolution of the population of the excited atomic state and the peak Rabi frequency, provided one knows the shape of the excitation pulse. One such time histogram is shown for a standard Gaussian pulse in fig. 4.11(a).

As seen from eqn. 4.16, the probability for the atom to decay within a time interval of length $\mathrm{d}t$ is proportional to the population of the excited state:

$$p\,\mathrm{d}t \propto |c_e|^2\,\mathrm{d}t \tag{4.36}$$

This quantity is directly related to the experimental arrival time histograms, since the number of events in a given time bin is proportional to the above probability. It does not give us the population inversion right away, because there is a constant, but unknown, scaling factor between these two quantities. Therefore we will use our knowledge of the pulse shapes to determine this factor and thus all other relevant quantities. The peak Rabi frequency and the scaling factor are used as free parameters in a fitting routine, which repeatedly solves the optical Bloch equations while varying the fit parameters such that the deviation of the evolution $|c_e|^2$ from the measured data is minimized. The result for the Gaussian pulse can be seen in fig. 4.11(b).

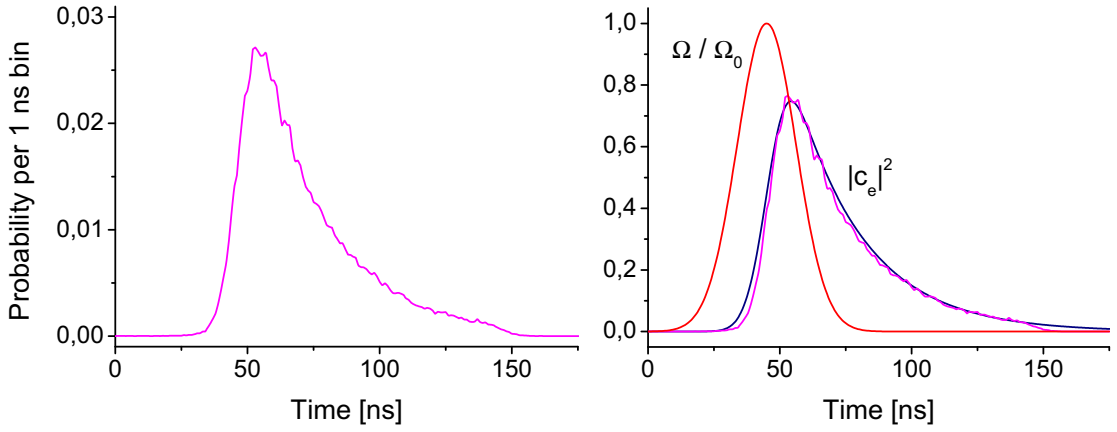

Figure 4.11: Arrival time histogram of the photons with a total number of 159577 photons. (a) Normalized probability to find a photon in a time bin of width 1 ns (b) Fit of the numerical simulation to the histogram assuming a Gaussian pulse with $\Delta t = 26.3\,\text{ns}$, from which the peak Rabi frequency $\Omega_0/2\pi = 25\,\text{MHz}$ can be inferred

Once the peak Rabi frequency is determined, the multi-photon emission probability can be calculated, according to eqn. 4.23. Tab. 4.1 shows the fit results for all four pulse forms. The experimentally observed multi-photon emission probabilities agree at least qualitatively with the calculated ratios for the rectangular pulses. The Gaussian form yields an even better result than numerically predicted. As to the sawtooth pulse, the theoretical value lies 2 orders of magnitude below the measured ratio. A possible reason for these discrepancies is our treatment of ^{87}Rb as an idealised two-level system, rather than an actual multi-level system. This matter will be discussed briefly in the next section.

Pulse form	FWHM Δt [ns]	$\Omega_0/2\pi$ [MHz]	p_m/p_1 (numerical)	p_m/p_1 (exp.)
Gaussian	26.3	25	$5.74 \cdot 10^{-1}$	$6.08 \cdot 10^{-2}$
Rectangular	15.2	30	$1.15 \cdot 10^{-1}$	$4.33 \cdot 10^{-2}$
Rectangular	6.05	50	$2.67 \cdot 10^{-2}$	$5.07 \cdot 10^{-2}$
Sawtooth	4.45	40	$5.56 \cdot 10^{-4}$	$3.46 \cdot 10^{-2}$

Table 4.1: Results of the fitting algorithm determining the peak Rabi frequency Ω_0. The subsequently numerically computed ratios p_m/p_1 (without considering dark count effects) can then be compared to the experimental values.

4.3 Multi-level effects

So far we have treated the ^{87}Rb atom in a simplified way, taking only two states into account, namely the $^2S_{1/2}\ |F=1, m_F=0\rangle$ ground state and the $^2P_{3/2}\ |F'=0, m_{F'}=0\rangle$ excited state. This is not a satisfying description, due to the fact that the atom can decay to different states than the one from which it was excited (see fig. 4.12).

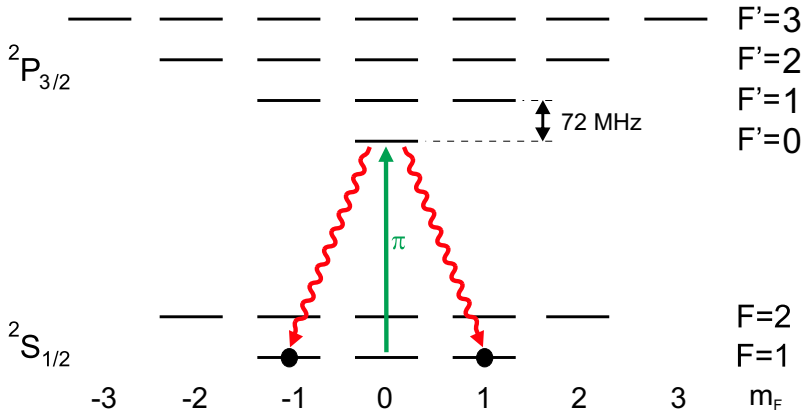

Figure 4.12: Complete level structure of ^{87}Rb for the D_2 transition. The atom is excited via a π transition and then decays to $^2S_{1/2}\ |F=1, m_F=+1\rangle$ and $|F=1, m_F=-1\rangle$, emitting σ^- and σ^+ light, respectively.

Let us assume perfect pumping to the $|F=1, m_F=0\rangle$ ground state. After exciting the atom with a π-polarized light pulse to the $|F'=0, m_{F'}=0\rangle$ state, it decays back to one of the $|F=1, m_F=\pm1\rangle$ states (the state $|F=1, m_F=0\rangle$ does not play a role, as we do not detect photons from this decay, cf. section 2.3.1). In theory, it should be impossible to re-excite the atom from one of these states, as there are no levels to which a π-polarized pulse could excite the atom. However, this scheme is thwarted by two mechanisms, imperfect polarization of the exciting light field and spectral broadening of the pulses.

Imperfect polarization

If the excitation light is partially circularly polarized, the atom can be re-excited from the $|F=1, m_F=\pm1\rangle$ states to $|F'=0, m_{F'}=0\rangle$, as this is no longer a forbidden transition. In order to prepare a good linear polarization of the excitation pulse, the beam axis must be aligned perpendicularly to the quantization axis. Any misalignment would result in a corresponding fraction of $\sigma^{\pm}$-polarization.

The experimental challenge of this approach is that there is no live signal to which the alignment can be adjusted. Each time the angle between the beam and quantization axis has been modified, an autocorrelation measurement must be performed, which usually requires several hours of measurement time. A perfectly π-polarized excitation pulse would then never induce the emission of a second photon. Hence, the pulse could be arbitrarily long, taking away the need to generate short excitation pulses. This would be very convenient, as it would also dramatically reduce the effect of spectral broadening which occurs for short pulses.

Spectrally broadened pulses

Introducing temporally short excitation pulses, the frequency spectrum of the pulse becomes broader. This is due to Heisenberg's energy-time uncertainty principle, giving rise to a lower bound for the bandwidth-time product of a light pulse. For a Gaussian shape, it is given by [39]

$$\Delta\nu\Delta t \geq 0.44, \tag{4.37}$$

where $\Delta\nu$ and Δt are the full widths at half maximum both in frequency and time domain. This means that for a given duration Δt of the pulse, the frequency spectrum has a certain minimum width, leading to the population of off-resonant upper states, such as $|F' = 1\rangle$. Given a short pulse with $\Delta t = 5\,\mathrm{ns}$, the bandwidth becomes sufficiently large with $\Delta\nu \geq 88\,\mathrm{MHz}$ to excite this state. Thus even a perfectly π-polarized excitation pulse can re-excite the atom after a decay to the $|F = 1, m_F = \pm 1\rangle$ ground states. Moreover, this effect diminishes the quality of atom-photon entanglement and the two-photon interference as the photons emitted by the atom can now be distinguished not only by their polarization but also their frequency.

Summary

In this chapter, a basic two-level model was developed to estimate the probability of multi-photon emissions by an atomic dipole driven by a pulsed light field. It was shown that the most important parameters of the light pulse to optimize in order to suppress unwanted multiple photons are the pulse duration and pulse area. Reducing the duration prevents the atom from emitting secondary photons, as the pulse is over after the first decay. Using a smaller pulse area, in contrast, is a promising way to realize a clean single-photon source.

Experimentally, we found that the rectangular excitation pulses do not give much improvement over the Gaussian shape. The sawtooth pulse, however, reduces the multi-photon to single-photon ratio, in particular when adjusting the time window such that only photons emitted after the end of the excitation pulse are accepted.

Two more points worth noting are polarization effects and spectral broadening of the excitation pulse which were not considered in the two-level model. Though experimentally difficult to achieve, a perfectly π-polarized pulse could suppress multi-photon events, even for long pulses. Short pulses are spectrally broadened and have thus the drawback of driving off-resonant transitions. This leads to photons of different frequency, reducing the fidelity of the entangled atom-photon state and therefore also the fidelity of the final entangled atom-atom state.

Chapter 5

Conclusion and Outlook

In this work, the quantum interference of a pair of single photons, which is a key element for creating entanglement between two spatially separated atoms, was investigated experimentally. The first step of this entangling protocol is to entangle each atom with a photon via spontaneous decay in a Λ-type atomic transition [23]. The emitted photons are then brought to interference on a 50/50 beam splitter. By coincidental detection of two photons in the output modes of the beam splitter, a Bell-state measurement of the joint photonic state is realized. Due to entanglement swapping, this measurement procedure projects the atoms onto an entangled state.

In order to observe a significant two-photon interference contrast, the impinging photons have to be indistinguishable in all degrees of freedom. We therefore synchronized independent excitation pulses in the two atom traps at a distance of 30 m with an accuracy of $\approx$ 1 ns. The quality of the two-photon interference was obtained by observing polarization-dependent two-photon cross-correlations. A measure for the interference quality is the ratio of theoretically forbidden simultaneous coincidences to those caused by a projection onto the Bell states $|\Psi^{\pm}\rangle$, which was found to be 0.159. This led us to the conclusion that the emitted photonic wave packets contain more than one photon each. Clearly, multiple photons emitted by the same atom can mimic actual two-photon interference events.

The problem of multi-photon emission was investigated in the last chapter. Such events can occur since the duration of the excitation pulse is on the order of the lifetime of the excited state. Consequently, the atom has a chance to decay and emit a photon before the pulse is over and there is a non-vanishing probability of re-exciting the atom, leading to a second photon. Using a Hanbury-Brown-Twiss setup, the fraction of multi-photon events from an excitation could be measured for excitation pulses of different shapes and durations. A sawtooth shaped pulse with a duration of $\approx$ 3 ns (FWHM in intensity) reduced the undesired multi-photon emission roughly by a factor of 2 compared to the Gaussian shape used before. We achieved a further improvement by discarding photons which were detected outside of a predefined time window. This ensured that only photons emitted by the atom after the end of the excitation pulse were accepted, leading to a value for the multi-photon probability comparable to what is expected from dark count events of the detectors. The experimental values were compared to a numerical simulation using the optical Bloch equations for a two-level system. In general, significant discrepancies between the experimental and numerical values were observed. Since ^{87}Rb has a multi-level structure, the two-level description does not take polarization effects and off-resonant

excitations by spectrally broadened pulses into account.

Outlook

The discussed methods for reducing the fraction of multi-photon emission during the atomic excitation are not sufficient, mainly because short pulses are spectrally broad and thus degrade the quality of the atom-photon entanglement. Hence, different techniques will be needed. One approach is to use a cavity for the scattered photons, filtering out photons from unwanted transitions. In order to achieve a high transmission for the photons from the transition $|F' = 0\rangle \rightarrow |F = 1\rangle$, the cavity resonance should have the same linewidth as the atomic transition (6.1 MHz). For an optimal suppression of photons from the level $|F' = 1\rangle$, a free spectral range of $2 \cdot 72\,\mathrm{MHz}$ is advisable. Since stability on the order of 1 MHz is required, the cavity needs to be actively stabilized to a reference laser.

Appendix A

Supplementary information

A.1 Spectrum and arrival time probability of single photons

The temporal shape of the wave packets in section 3.1.4 was given as

$$\chi(t) = \frac{1}{\sqrt{\tau}} e^{-\frac{1}{2}\frac{t-t_0}{\tau}} \Theta(t-t_0)\, e^{-i\omega_0 t}. \tag{A.1}$$

We are interested in the frequency spectrum of this light field. Following eqn. 3.7, we find the following spectrum amplitude for above shape:

$$\chi(\omega) = \frac{1}{\sqrt{2\pi}} \int \chi(t)\, e^{i\omega t}\, \mathrm{d}t \tag{A.2}$$

$$= -\sqrt{\frac{2\,\tau}{\pi}} \frac{e^{i(\omega-\omega_0)t_0}}{2i\,(\omega-\omega_0)\,\tau - 1} \tag{A.3}$$

The probability density of the frequency spectrum is then given by

$$|\chi(\omega)|^2 = \frac{1}{\pi} \frac{\tau}{2\,(\omega-\omega_0)^2\,\tau^2 + 1}, \tag{A.4}$$

which is a Lorentzian function, as expected for an exponential decay in the time domain (see fig. A.1(a)). The FWHM of the distribution function is $\sqrt{2}/\tau = 2\pi \cdot 8.58\,\mathrm{MHz}$, which is, as expected, related to the lifetime of the excited state of the D_2 transition of ^{87}Rb.

Another point worth noting is the probability to detect two photons at two different points in time. This is not connected to any interference effects, we merely consider two perfectly overlapped wave packets impinging on an ideal single-photon detector (i.e. unit quantum efficiency and no dead-time). The probability for detecting two photons at times t_1 and t_2 is found to be

$$p\,\mathrm{d}t_1\mathrm{d}t_2 = |\chi(t_1)|^2\,|\chi(t_2)|^2\,\mathrm{d}t_1\,\mathrm{d}t_2. \tag{A.5}$$

As we are only interested in the time difference $\delta t = t_2 - t_1$, we can integrate over one time variable:

$$p\,\mathrm{d}(\delta t) = \mathrm{d}(\delta t) \int |\chi(t)|^2\,|\chi(t+\delta t)|^2\,\mathrm{d}t \tag{A.6}$$

$$= \frac{1}{2\,\tau} e^{-\frac{|\delta t|}{\tau}}\,\mathrm{d}(\delta t) \tag{A.7}$$

This means that large detection time differences are exponentially unlikely, as can be seen in fig. A.1(b).

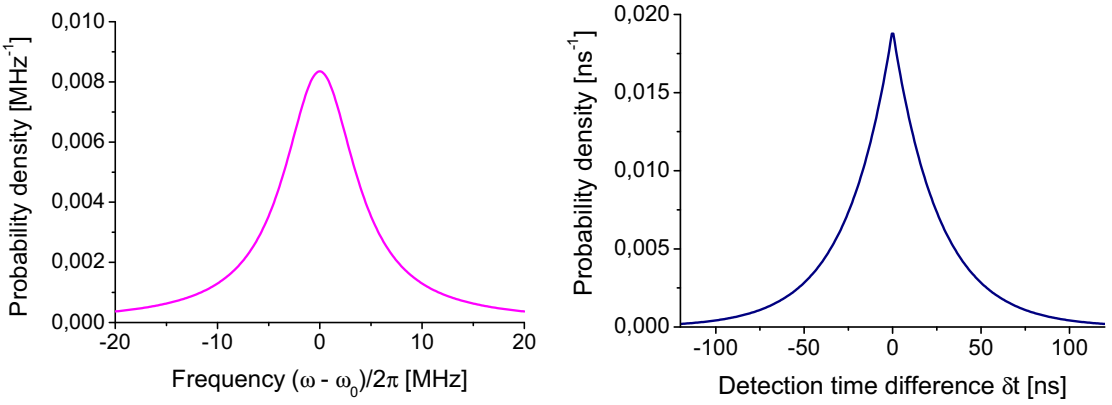

(a) (b)

Figure A.1: (a) Frequency spectrum of the photonic wave packets given by their temporal shape $\chi(t)$ (b) Probability density distribution of the time difference δt between the detection of two photons with overlapped wave packets

A.2 Multi-photon emission simulation

As derived in section 4.1.2, the probability for an atom driven by an external light field to emit more than one photon is given by

$$p_m(t) = 1 - p_0(t) - p_1(t). \tag{A.8}$$

The zero-photon emission probability $p_0(t)$ is given by a simple time integral (eqn. 4.18). However, a difficulty arises when trying to evaluate the single-photon probability (eqn. 4.22):

$$p_1(t) = \int_{-\infty}^{t} p_0(-\infty, t')\,\Gamma\left|c_e(t')\right|^2 p_0(t', \infty)\,\mathrm{d}t' \tag{A.9}$$

$$= \int_{-\infty}^{t} \Gamma\left|c_e(t')\right|^2 \exp\left(-\int_{-\infty}^{t'} \Gamma\left|c_e(t'')\right|^2 \mathrm{d}t'' - \int_{t'}^{\infty} \Gamma\left|c_e(t'')\right|^2 \mathrm{d}t''\right) \mathrm{d}t' \tag{A.10}$$

At first glance, it seems the two integrals in the exponential can be combined to a single integral ranging from $-\infty$ to ∞. One must note, unfortunately, that at time t', the quantum jump takes place. This means that for the first integral, the atom undergoes a coherent evolution, which it *does not* continue for the second integral, but instantly decays to the ground state at t' from where it resumes its coherent evolution.

Hence, we have the problem that the limits of the two inner integrals depend on the outer integration variable. When numerically solving this expression, the computing time scales quadratically with the number of time steps. Depending on the accuracy needed, this results in a processing time of one to several hours. It becomes even more dramatic when varying parameters like the pulse duration or pulse area, as the calculation of $p_1(t)$ must now be done 50 to 100 times, resulting in total computing times of several days.

Approximation to the coherent evolution

For arbitrary excitation pulses, the two inner integrals in eqn. A.10 must be solved numerically. For rectangular pulses, on the other hand, the coherent evolution, and thus its integral, is given analytically for any time and any initial state. For example, for a system starting in the ground state, a light field on resonance ($\delta = 0$) causes oscillations of the upper state population:

$$|c_e(t)|_i^2 = \frac{1}{2}(1 - \cos(\Omega_i t)) \quad (A.11)$$

$$= \sin^2\left(\frac{\Omega_i t}{2}\right) \quad (A.12)$$

Here Ω_i is the mean Rabi frequency over the i-th interval. For detuning and arbitray initial states, this expression becomes more complicated, involving also the coherence c_{ge} of the system. The approach to reduce the numerical cost for solving eqn. A.10 is to divide the Rabi pulse into several equally spaced intervals in time. In each of the intervals, the Rabi frequency is assumed to be constant and given by the average of the original Rabi frequency over the respective interval. This means that for a given time, the coherent evolution can be calculated by adding up the evolution in each of the preceding rectangles. By that, the total computational cost can be reduced from a quadratic dependence on the number of time steps to a linear dependence on the time steps and the intervals.

Typical values are 50000 for the time steps and 50 for the intervals, thus reducing the numerical cost by roughly 3 orders of magnitude. An example of this technique is shown in fig. A.2 for a Gaussian pulse being divided into only 3 rectangular pulses. For such a small number of intervals, deviations of the coherent evolution from the exact values are noticeable, but for a number as large as 50, these can be neglected.

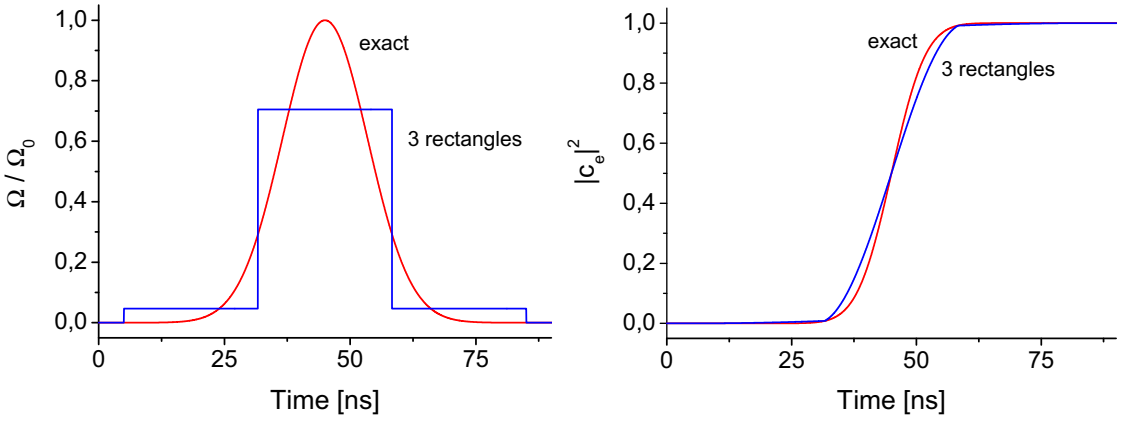

(a) (b)

Figure A.2: Analytic approximation of a Gaussian pulse by 3 rectangular pulses. (a) Each Rabi frequency is chosen as the arithmetic mean of the actual Rabi frequency over the respective time interval, preserving the pulse area. (b) Comparison between the exact and the analytic values of the coherent evolution. A deviation is visible, due to the very small number of intervals.

Bibliography

[1] Abdus Salam. *Unification of Fundamental Forces*. Cambridge University Press, 1990.

[2] A. Einstein, B. Podolsky, and N. Rosen. Can Quantum-Mechanical Description of Physical Reality Be Considered Complete? *Phys. Rev.*, 47:777, 1935.

[3] W. Heisenberg. Über den anschaulichen Inhalt der quantentheoretischen Kinematik und Mechanik. *Zeitschrift für Physik A*, 43:172, 1927.

[4] J. S. Bell. On the Einstein-Podolsky-Rosen Paradox. *Physics*, 1:195, 1964.

[5] S. J. Freedman and J. F. Clauser. Experimental Test of Local Hidden-Variable Theories. *Phys. Rev. Lett.*, 28:938, 1972.

[6] A. Aspect, P. Grangier, and G. Roger. Experimental Tests of Realistic Local Theories via Bell's Theorem. *Phys. Rev. Lett.*, 47:460, 1981.

[7] P. H. Eberhard. Background level and counter efficiencies required for a loophole-free Einstein-Podolsky-Rosen experiment. *Phys. Rev. A*, 47:R747, 1993.

[8] G. Weihs, T. Jennewein, C. Simon, H. Weinfurter, and A. Zeilinger. Violation of Bell's Inequality under Strict Einstein Locality Conditions. *Phys. Rev. Lett.*, 81:5039, 1998.

[9] D. N. Matsukevich, P. Maunz, D. L. Moehring, S. Olmschenk, and C. Monroe. Bell Inequality Violation with Two Remote Atomic Qubits. *Phys. Rev. Lett.*, 100:150404, 2008.

[10] M. A. Rowe, D. Kielpinski, V. Meyer, C. A. Sackett, W. M. Itano, C. Monroe, and D. J. Wineland. Experimental violation of a Bell's inequality with efficient detection. *Nature*, 409:791, 2001.

[11] M. Zukowski, A. Zeilinger, M. A. Horne, and A. K. Ekert. "Event-ready-detectors" Bell experiment via entanglement swapping. *Phys. Rev. Lett.*, 71:4287, 1993.

[12] W. Rosenfeld, M. Weber, J. Volz, F. Henkel, M. Krug, A. Cabello, M. Zukowski, and H. Weinfurter. Towards a Loophole-Free Test of Bell's Inequality with Entangled Pairs of Neutral Atoms. *Adv. Sci. Lett.*, 2:469, 2009.

[13] J. Volz, M. Weber, D. Schlenk, W. Rosenfeld, J. Vrana, K. Saucke, C. Kurtsiefer, and H. Weinfurter. Observation of Entanglement of a Single Photon with a Trapped Atom. *Phys. Rev. Lett.*, 96:030404, 2006.

[14] W. Rosenfeld, F. Hocke, F. Henkel, M. Krug, J. Volz, M. Weber, and H. Weinfurter. Towards Long-Distance Atom-Photon Entanglement. *Phys. Rev. Lett.*, 101:260403, 2008.

[15] Michael Krug. Atomic traps for efficient state detection of a single atom. Master's thesis, Ludwig-Maximilians-Universität München, 2007.

[16] Norbert Ortegel. Atom-Photon Entanglement. Master's thesis, Ludwig-Maximilians-Universität München, 2009.

[17] Michael A. Nielsen and Isaac L. Chuang. *Quantum Computation and Quantum Information*. Cambridge University Press, 2000.

[18] Franz Schwabl. *Quantenmechanik*. Springer-Verlag, 1990.

[19] S. J. van Enk, N. Lütkenhaus, and H. J. Kimble. Experimental procedures for entanglement verification. *Phys. Rev. A*, 75:052318, 2007.

[20] Dirk Bouwmeester, Artur Ekert, and Anton Zeilinger. *The Physics of Quantum Information*. Springer-Verlag, 2000.

[21] M. Weber, J. Volz, and K. Saucke. Analysis of a single-atom dipole trap. *Phys. Rev. A*, 73:043406, 2006.

[22] D. A. Steck. Rubidium 87 D Line Data. *Available online at http://steck.us/alkalidata*, 2009.

[23] Jürgen Volz. *Atom-Photon Entanglement*. PhD thesis, Ludwig-Maximilians-Universität München, 2006.

[24] Markus Weber. *Quantum optical experiments towards atom-photon entanglement*. PhD thesis, Ludwig-Maximilians-Universität München, 2005.

[25] Mark Fox. *Quantum Optics*. Oxford University Press, 2006.

[26] C. Schuck, G. Huber, C. Kurtsiefer, and H. Weinfurter. Complete Deterministic Linear Optics Bell State Analysis. *Phys. Rev. Lett.*, 96:190501, 2006.

[27] J. F. Clauser, M. A. Horne, A. Shimony, and R. Holt. Proposed Experiment to Test Local Hidden-Variable Theories. *Phys. Rev. Lett.*, 23:880, 1969.

[28] P. M. Pearle. Hidden-Variable Example Based upon Data Rejection. *Phys. Rev. D*, 2:1418, 1970.

[29] Florian Henkel. Private communication.

[30] Fredrik Hocke. Long Distance Atom Photon Entanglement. Master's thesis, Ludwig-Maximilians-Universität München, 2007.

[31] Marlan O. Scully and M. Suhail Zubairy. *Quantum Optics*. Cambridge University Press, 1997.

[32] C. K. Hong, Z. Y. Ou, and L. Mandel. Measurement of subpicosecond time intervals between two photons by interference. *Phys. Rev. Lett.*, 59:2044, 1987.

[33] T. Legero, T. Wilk, M. Hennrich, G. Rempe, and A. Kuhn. Quantum Beat of Two Single Photons. *Phys. Rev. Lett.*, 93:070503, 2004.

[34] C. Kurtsiefer. A programmable pattern generator. *Unpublished*.

[35] Wenjamin Rosenfeld. Private communication.

[36] Julian Hofmann. Private communication.

[37] Benoît Darquié. *Manipulation d'atomes dans des pièges dipolaires microscopiques et émission contrôlée de photons par un atom unique*. PhD thesis, Université Paris XI, 2005.

[38] R. Hanbury Brown and R. Q. Twiss. Correlation between Photons in two Coherent Beams of Light. *Nature*, 177:27, 1956.

[39] T. L. Koch and J. E. Bowers. Nature of wavelength chirping in directly modulated semiconductor lasers. *Electron. Lett.*, 20:1038, 1984.

Danksagung

Ich möchte allen danken, die mich während des vergangenen Jahres unterstützt und zum Gelingen dieser Arbeit beigetragen haben:

- Harald Weinfurter, für die freundliche Aufnahme in seine Arbeitsgruppe und die große Freiheit, die er seinen Leuten bei der Arbeit lässt
- Markus Weber, der immer ein offenes Ohr für Probleme und Anregungen hat, für seine Rolle als Betreuer und Ansprechpartner während meiner Zeit an diesem Projekt
- Wenjamin Rosenfeld, für seine Bereitschaft, bei Fragen stets schnell und unkompliziert weiterzuhelfen
- Michael Krug, für die Zeit beim Justieren und Messen und seine Freude am Erklären von physikalischen Sachverhalten
- Julian Hofmann, für die Einführung in das Experiment und die Unterstützung bei technischen Fragen
- Florian Henkel, für die kulinarische Verpflegung während der Gruppensitzungen
- Dem gesamtem Weinfurter-Team, in dem eine freundliche und stimulierende Arbeitsatmosphäre herrscht
- Andreas Jöckel, der mir ein angenehmer und hilfsbereiter Bürokollege war
- Eric Deal, für die sprachliche Korrektur dieser Arbeit
- Meinen Eltern, für die Möglichkeit, dieses Studium aufnehmen zu können und für die moralische Unterstützung in schwierigen Zeiten